CHAPTER 4

EVALUATION OF THE COMPRESSION PERFORMANCE OF REC ECHOES USING A SPATIALLY VARYING WIENER FILTER

4.1 Introduction

The focus of the chapter is to evaluate techniques that improve the image quality using a coding and pulse compression technique by either reducing the sidelobe levels, improving spatial resolution, or increasing the signal-to-noise ratio beyond what is available when using a Wiener filter. The techniques evaluated in this chapter were applied directly to the REC technique but could also be applied to general techniques involving coded excitation and pulse compression. In previous chapters, compression was based on the simplification that the spatially varying nature of the echo signals was negligible. Under this simplification, the Wiener filter used for compression did not include a spatially varying response. However, it was hypothesized that a Wiener filter containing adaptive variables based on the spatial location of the region being evaluated would lead to improved image quality. Simulations and experiments were conducted to test the hypothesis.

This chapter is subdivided into two sections, with each section evaluating a different variable being adjusted in the Wiener filter. The first section will evaluate the effects on the compression when the adjustable parameter in the Wiener filter is the linear chirp that depends on the spatially varying pulse-echo impulse response. The second section will evaluate the effects on the compression when the adjustable parameter is the spatially varying echo-signal-to-noise ratio.

4.2 Spatially Varying Wiener Filter with a Spatially Varying Linear Chirp Parameter

In the original design of the pre-enhanced chirp, the overall system impulse response was approximated by the impulse response of the source measured at the focus. In other words, a non-spatially-varying impulse response of the transducer was assumed. When imaging targets that were not located at the focus, a mismatch between the transmitted signal that had been optimized for the focus and the received echo could occur. Therefore, because of the assumption that the impulse response did not vary spatially, the compression performance away from the focus was hindered because sidelobe levels were observed to increase and a loss of axial resolution occurred.

In this subsection, the effects of the spatially varying nature of the impulse response were evaluated. In addition, techniques to compensate for the spatial impulse response in the compression scheme (Wiener filter) were examined. The overall objective was to remove any system dependencies in order to make all compressed echoes throughout the depth of field behave as if they were imaged at the focus of the source.

4.2.1 Spatial impulse response

In ultrasound, the overall system response can be described symbolically as follows:

$$g(x,y,z,t) = e(t) * emir_t(t) * sir_t(x,y,z,t) * sir_r(x,y,z,t) * emir_r(t) \tag{4.1}$$

where t is the range time; x, y, and z are the spatial coordinates; $g(x,y,z,t)$ is the echo waveform; $e(t)$ is the excitation signal; $emir_t(t)$ and $emir_r(t)$ are the transmit and receive electromechanical impulse responses of the transducer; and $sir_t(x,y,z,t)$ and $sir_r(x,y,z,t)$ are the transmit and receive spatial impulse responses. The spatial impulse response is defined as the pressure wave radiated from a point at some location in space resulting from the velocity of the aperture [102–104]. The spatial impulse response [103] is described by the following expression:

$$sir(x,y,z,t) = \int_\sigma \frac{\delta(t - \frac{|\vec{r}-\vec{r_0}|}{c})}{2\pi|\vec{r}-\vec{r_0}|} dS, \tag{4.2}$$

where t is time, $\vec{r}_0$ is the position on the source (Fig. 4.1), $\vec{r}$ is the position of the field point of interest, σ is the area of the source, and S the surface of the source.

The expression in (4.2) uses the Rayleigh integral, which is valid for a piston source. However, for a weakly-focused source the Rayleigh integral is still valid and provides an excellent approximation [105–107]. Therefore, at the focal point of a focused transducer the pressure waves from all the points on the transducer surface arrive at approximately the same time and as a result the spatial impulse response is represented by a δ-function in time. This is shown in the Field II simulation [108, 109] in Fig.4.2. Field II is a software package that can be used in conjunction with MATLAB to simulate ultrasound transducer fields and to perform imaging of phantoms. Field II uses the concept of the spatial impulse response as described by Tupholme-Stepanishen [102–104] to calculate linear fields. Therefore, the symbolic expression in (4.1) at the focus reduces to

$$g(x, y, z, t) = e(t) * emir_t(t) * emir_r(t). \tag{4.3}$$

The spatial impulse response before (Fig. 4.3) and after (Fig. 4.4) the focus behaves like a low-pass filter, although the spatial impulse response changes more slowly after the focus.

In the development of the REC technique, the compression was achieved throughout the depth of field of a source by assuming the spatial impulse response was constant or non-spatially-varying. The pre-enhanced chirp was obtained by convolution equivalence [18] as follows:

$$V_{pre}(f) = V_{lin}(f) \times \frac{H_2(f)}{H_1(f)}. \tag{4.4}$$

The pre-enhanced chirp as constructed in (4.4) was optimized for imaging targets at the focus of the source. As the target moves away from the focus, in either direction, the spatial impulse response is no longer a δ-function, which changes the characteristics of the echo and as a result deteriorates the quality of the compression due to this mismatch. To prevent a mismatch, the pre-enhanced chirp could be designed for each spatial location as follows:

$$V_{pre}(f, x) = V_{lin}(f, x) \times \frac{H_2(f, x)}{H_1(f, x)}. \tag{4.5}$$

However, while such a solution is feasible, the tradeoff is that multiple excitations would reduce the imaging frame rate. In certain applications this is not desirable. An alternative would be to compensate for these spatially varying changes in the compression or the receive stage rather than in the transmission of the excitation signal. In this scenario H_2 is kept constant throughout x.

In the compression of REC echoes, a modified linear chirp, $V'_{lin}(f)$, is generated in order to restore convolution equivalence and obtain a better match between the MATLAB generated linear chirp, $V_{lin}(f)$, and the actual received echo. Previously, $V'_{lin}(f)$ was generated by the expression in (1.3). However, to compensate for the spatially varying nature of the impulse response, (1.3) was modified as follows:

$$V'_{lin}(f,x) = \frac{H_2^*(f)}{|H_2(f)|^2 + |H_2(f)|^{-2}} \cdot H_{out}(f,x), \tag{4.6}$$

where $H_{out}(f,x)$ represents echoes from a planar reflector obtained as a reference at different axial locations x within the depth of field. The hypothesis is that these references would result in improved compression because the references more closely follow (4.1), i.e., they include the spatial impulse response corresponding to the spatial location of the target. Therefore, by having multiple references generated at various locations throughout the depth of field, a spatially varying Wiener filter could be constructed:

$$\beta_{REC}(f,x) = \frac{V'^*_{lin}(f,x)}{|V'_{lin}(f,x)| + \gamma \overline{eSNR}^{-1}(f)}. \tag{4.7}$$

4.2.2 Experimental setup

Experiments were performed to test the spatially varying Wiener filter compression scheme. A single-element weakly focused (f/2.66) transducer (Panametrics, Waltham, MA) with a center frequency of 2.25 MHz and a 50% (at -3-dB) fractional bandwidth was used. These parameters were measured using the wire technique [97] for transducer characterization. The experimental setup utilized is described as follows:

The pre-enhanced chirp was generated in MATLAB and downloaded to an arbitrary waveform generator (Tabor Electronics W1281A, Tel Hanan, Israel). The excitation signal was amplified by a radio frequency power amplifier (ENI 2100L, Rochester, NY).

The amplified signal (50 dB) was connected to the transducer through a diplexer (Ritec RDX-6, Warwick, RI). The echo signal was received by a pulser-receiver (Panametrics 5800, Waltham, MA), which was displayed on an oscilloscope (Lecroy 9354 TM, Chester Ridge, NY) for visual verification. The echo signal was recorded at a rate of 200 MHz by a 14-bit analog-to-digital converter (Signatec PDA14-200, Newport Beach, CA) for further processing by a PC.

Measurements from a Plexiglas planar reflector, a 100 μm tungsten wire target surrounded by degassed water and a 120 μm nylon wire in a urethane rubber material were obtained to evaluate the compression performance of the spatially varying Wiener filter (4.7) vs. the conventional Wiener filter in (1.2). At a minimum, measurements were obtained for objects placed at the focus and at the depths before and after where the pressure amplitude was 6 dB below the focus.

4.2.3 Image quality metrics

To substantiate the improvements in the performance of the spatially varying Wiener filter, the following imaging quality metrics were used:

1. Sidelobe-to-mainlobe ratio (SMR): See Sec. 2.1.2 for more information.

2. Modulation transfer function (MTF): See Sec. 2.1.2 for more information.

4.2.4 Results

Planar reflector study

Experimental measurements from a planar reflector were obtained in increments of a wavelength throughout the depth of field. The resulting echoes were compressed using two methods: Compression with the conventional Wiener filtering with a $V_{lin}^{'}(f)$ reference from the focus as outlined by Oelze [18] and compression with a spatially varying Wiener filter that accounted for spatially varying $V_{lin}^{'}(f,x)$ references.

A snapshot of a few of the results highlighting the whole depth of field are displayed in Fig. 4.5. Note that in Fig. 4.5(a-c) multiple reflections from the planar reflector were visible and were only included to show the whole extent of the depth of field. The

results in Fig. 4.5(a) indicated that a maximum reduction in the sidelobe levels of 15 dB for the spatially varying Wiener filter was achieved. However, the average reduction in sidelobe levels when using the spatially varying Wiener filter was 10 dB. As the target approached the focus, Fig. 4.5(b), the reduction in sidelobe levels when using the spatially varying Wiener filter decreased with the maximum reduction at 13 dB and the average reduction at 8 dB. Furthermore, for targets closer to the focus, as shown in Fig. 4.5(c), the sidelobe levels for the spatially varying Wiener filter decreased with the maximum reduction at 10 dB and the average reduction of 5 dB. The echoes for both filters, the conventional Wiener filter and the spatially varying Wiener filter, should provide the same result when at the focus because the references used for compression were the same. This result is verified in Fig. 4.5(d). The results in Fig. 4.5(e-g) show the compression results when the target was located after the focus. Overall, the results in Fig. 4.5 suggest that the SVWF was more helpful at reducing the sidelobe levels as the target moved away from the focus.

Spatial resolution estimates based on the MTF for the plots in Fig. 4.5 are shown in Table 4.1. As expected, the spatial resolution when compressing with the Wiener filter and the spatially varying Wiener filter at the focus were the same, i.e., 302 μm. Moreover, when compressing targets outside the focus with the spatially varying Wiener filter, the spatial resolution estimates were consistently around the same spatial resolution value as the focus. When using the conventional Wiener filtering scheme, the spatial resolution estimates outside the focus degraded compared to the estimates at the focus. When using the conventional Wiener filter, the axial resolution deteriorated by 45% for the target located prior to the focus at the edge of the -6 dB depth of field. In addition, the axial resolution using the conventional Wiener filter at the same location was actually 2% worse than the axial resolution of CP. For the spatially varying Wiener filter, a gain of 43% in spatial resolution was obtained at the same location when compared to REC compressed with a conventional Wiener filter. These results suggest that the spatially varying Wiener filter was able to make all targets within the depth of field appear as if the target was being imaged at the focus. Therefore, the spatially varying Wiener filter improved the compression performance by increasing the axial resolution and decreasing sidelobe levels for the planar reflector target.

Tungsten wire targets

Experimental measurements of ultrasonic backscatter from a 100 μm tungsten wire were obtained at the focus and at the edges of the -6 dB depth of field. The resulting echoes were compressed using two methods: compression with the conventional Wiener filtering and compression with a spatially varying Wiener filter. While the imaging target was a wire, the reference waveforms for compression were taken from a planar Plexiglas plate.

The compressed images for wire targets at various locations in the -6 dB depth of field are shown in Figs. 4.6-4.8. When compressing signals from the edges of the depth of field with the spatially varying Wiener filter an increase in the eSNR of almost 5 dB was achieved compared to the conventional Wiener filter. In terms of sidelobe levels and spatial resolution, no significant improvements were obtained using qualitatively visual inspection of Figs. 4.6-4.8(a).

To get a better picture of the sidelobes, the on-axis plots in Figs. 4.6-4.8(b) were evaluated with quantitative metrics. The SMR for the long-range sidelobe were reduced by 3 to 5 dB in some locations while increases of 2 to 8 dB were observed in other locations. Similar increases were observed for the short-range sidelobes. Spatial resolution estimates based on the MTF for the plots in Fig. 4.6-4.8 are tabulated in Table 4.2. As expected, the spatial resolution values when compressing with the conventional Wiener filter and the spatially varying Wiener filter at the focus were the same, i.e., 426 μm. However, estimates of spatial resolution away from the focus were not as promising when using the spatially varying Wiener filter scheme for the wire targets. Examination of the spatial resolution estimated for points outside the focus revealed that the conventional Wiener filtering yielded better results for the wire target than the spatially varying Wiener filter.

The conclusion drawn from the the planar reflector study was that the spatially varying Wiener filter was helpful at improving the performance of the compression when the target was the same as the reference. However, for the wire target study, improvements were not observed in the spatial resolution and were marginal in the reduction of sidelobes and gain in eSNR. The system-dependent effects were partially compensated by using the spatially varying Wiener filter and compressing with references obtained at

the same spatial location as the target being imaged. Therefore, the main differences between the two studies were the shape and material of the imaging targets. Specifically, the scattering functions between the two targets were different because the collection of spatial impulse responses on the surface of the target were different. The scattering function for an object is related to the summation of the spatial impulse response of the field across the surface of the object.

To illustrate the collection of spatial impulse responses corresponding to the surface of an object more carefully, Field II simulations [108,109] of a planar reflector and a wire target were generated. The planar reflector and the wire target are continuous objects that were discretized in MATLAB as a collection of points, as shown in Fig. 4.9. The planar reflector was 10 mm wide and 10 mm high with grid points separated by 50 μm, which is much smaller than a wavelength. The wire was 150 μm wide and 10 mm high with grid points separated by 50 μm. For each grid point a spatial impulse response was calculated. The contribution of the spatial impulse responses or the sum is shown in the Field II simulation [108, 109] in Fig. 4.10.

The results in Fig. 4.10 suggest that a significant mismatch existed between references obtained from a planar reflector and the optimal filter design for the wire target. Therefore, it is hypothesized that for optimal compression the scattering function, which is related to the summation of spatial impulse responses incident on the target, should be taken into account. However, in a real imaging scenario only the spatial impulse response and the scattering function related to the reference geometry, i.e., planar reflector, are known. For the case of the planar reflector study, the imaging target was a planar reflector while the references were also from a planar reflector. Consequently, the improvements observed in the planar reflector study were due to "self-compression." Self-compression is the act of compressing echo signals with references made from the same object. With self-compression, both the collection of spatial impulse responses and the scattering function of the imaging object are compensated upon compression. Therefore, to further validate this hypothesis, the wire target's echoes were self-compressed (i.e., instead of using planar reflector references as usual, references were made from tungsten wire targets located at the same depth being imaged).

The self-compressed images for wire targets located at the edges of the -6 dB depth

of field are shown in Figs. 4.11-4.12(a). In the self-compressed cases, there were no improvements observed in eSNR similar to the gains observed using a spatially varying Wiener filter with a planar reflector as a reference. At first glance at Figs. 4.11-4.12, it would appear that noise was boosted. However, the apparent increase in noise is explained by the increase in the sidelobe levels slightly above the dynamic range of the imaging system. Overall, the sidelobe levels appeared to decrease in the self-compressed images when compared to the conventional compression scheme. In fact, the sidelobes were barely above the -50 dB amplitude level for both self-compressed cases as shown in the on-axis plots in Figs. 4.11-4.12(b). A significant improvement in the long-range sidelobe levels was observed when compared to the spatially varying Wiener filtering case when compressing with a planar reflector as a reference. For the self-compressed scenario where the reference was obtained at the same spatial location the target was imaged, the long range sidelobes were reduced by 5 dB in some locations and increased by about 2 dB in others. Overall there was a net reduction in sidelobe levels. In terms of the short-range sidelobe levels, a maximum reduction of 12 dB was observed. The short-range sidelobes were contained within the mainlobe of the conventional compression cases (planar reflector reference), which suggests that the self-compressed case had improved axial resolution.

Spatial resolution values obtained by evaluating the MTF for the targets plotted in Fig. 4.11-4.12 are listed in Table 4.2. The MTF results indicated that self-compression provided significant improvement in terms of axial resolution compared to compression with a planar reflector reference. For the self-compressed scattered signal, the axial resolution at the edge of the -6 dB depth of field prior to the focus improved by 26%. At the edge of the -6 dB depth of field after the focus, the improvement in axial resoltuion was 14%. Compared to CP, the improvements were 68% and 23%, respectively. These results suggested that by using a self-compressed spatially varying Wiener filter (wire target as a reference) not only were system effects partially compensated for, but target-dependent effects were also taken into account.

In summary, four compression scenarios were evaluated with the wire target:

1. Conventional Wiener filtering with the reference from a planar reflector obtained at the focus of the source. Results are shown in blue in Figs. 4.7(b) and 4.8(b).

This result did not compensate for spatially varying field effects or scattering.

2. Spatially varying Wiener filtering with the reference off of a planar reflector obtained at the same spatial location at which the target was located. Results are shown in green in Figs. 4.7(b) and 4.8(b). This result compensated for spatially varying field effects but not scattering.

3. Conventional Wiener filtering with the reference obtained from a wire located at the focus of the source. Results are shown in blue in Figs. 4.11(b) and 4.12(b). This result compensated for the scattering of the wire but not for the spatially varying effects.

4. Spatially varying Wiener filtering with the reference off of a wire target obtained at the same spatial location that the target was located. Results are shown in green in Figs. 4.11(b) and 4.12(b). This result compensated for both spatially varying effects and scattering.

The best results were achieved under scenario four as it reduced sidelobe levels and improved the axial resolution. Nonetheless, the results in scenario four pose a problem as it may potentially suggest that more than the system-dependent information must be known in order to significantly improve the compression performance. Specifically, information about the frequency dependent scattering from the object function must be known to account for scattering-dependent compression effects. Unfortunately, in most imaging scenarios this information is not given.

Nylon wire targets in the ATS phantom

Experimental measurements of a 120 μm nylon wire target inside the ATS tissue-mimicking phantom were obtained. The targets were imaged at the focus and at the edge of the -6 dB depth of field prior to the focus.

The compressed images for the target located at the focus are shown in Fig. 4.13(a). These images are shown as a reference for comparison because they are the gold standard for the entire depth of field. The compressed images for the target located prior to the focus are shown in Fig. 4.14(a). In Fig. 4.14(a) it was observed qualitatively that the spatially varying Wiener filter obtained a slightly better image in some regions where

the image appeared more crisp; however, sidelobes beyond the target appeared to have been accentuated. Although the sidelobe levels appeared higher for the spatially varying Wiener filter case, it was hard to assess the sidelobe levels in this scenario because the speckle due to subresolution scatterers may have compressed with more efficiency than the nylon wire target (i.e., the bandwidth matched the speckle response more for the spatially varying Wiener filter). Therefore, a significant roadblock exists to quantifying the sidelobe levels from these results. Furthermore, the ATS phantom images contain speckle in the background as opposed to a wire target in water. Therefore, the significant improvements in sidelobe levels could be buried beneath the speckle floor. Hence, only improvements in the axial resolution could be directly quantified.

For the ATS phantom results, instead of using MTF to obtain an estimate of spatial resolution, the more appropriate metric of speckle correlation length [32] was used. When compressing with the Wiener filter and the spatially varying Wiener filter, the speckle correlation lengths were estimated to be equal, i.e., 200 μm. For CP the correlation length was 606 μm. These results indicated that there were no significant differences between compressing REC echoes with a conventional Wiener filter and spatially varying Wiener filter.

In addition, the ATS data was compressed with references from a tungsten wire. The idea is that these references, although not made out of nylon, are still cylindrical in shape and would partially remove the scattering-dependent effects due to the wires and provide improved compression performance as observed with the tungsten wire targets. There were two scenarios studied: one using a tungsten wire located at the focus of the source as a reference. In this case, the effects of scattering were partially considered, but the spatially varying effects due to diffraction were not. The other scenario used a tungsten wire reference from the same spatial location at which the target was located. Therefore, both the spatially varying effect due to diffraction and scattering were partially taken into account.

The images of the target located at the edge of the -6 dB depth of field and compressed with a tungsten wire target reference are shown in Fig. 4.15(a). The speckle in the conventional Wiener filtering case appeared similar to the speckle in the CP case. This similarity in speckle would suggest that the axial resolution gain from using a pre-

enhanced chirp with REC was diminished. This similarity in speckle may have occurred because of a mismatch in the spectral content between the echo data and the reference. However, upon evaluating the on-axis plot in Fig. 4.15(b), a loss in resolution was not observed when comparing images produced with the conventional Wiener filter to the spatially varying Wiener filter. For images produced with the spatially varying Wiener filter case, the portion of the image near the target appeared to be slightly blurry. Similarly, the width of sidelobes for the spatially varying Wiener filter in Fig. 4.15(b) appeared slightly wider, indicating some loss in axial resolution. The spatial resolution as determined by the speckle correlation length for the conventional Wiener filter case was 266 μm. For the conventional Wiener filter case, the speckle correlation length increased by 29% when the reference changed from a planar reflector to a tungsten wire target. For the spatially varying Wiener filter, the spatial resolution as determined by the correlation length was 200 μm. In terms of sidelobes, the spatially-varying wiener filter (wire reference) appeared to have a lower amplitude level compared to using a planar reflector reference. Moreover, there was a decrease in the mainlobe amplitude. The decrease in mainlobe amplitude resulted from a difference in echo amplitude level between the planar reflector and wire target reference. Overall, compressing with a wire added what appeared to be sidelobes by an average of 6 dB when compared to the case when the references were planar reflectors. Overall, the spatially varying Wiener filter when the reference was a tungsten wire target did not add any benefits to the compression performance.

Finally, for completion of the study, the ATS data was self-compressed with references obtained from the nylon wire targets inside the ATS phantom. Because echoes from wire target were stronger than the background, careful extraction of the reference was possible so that information from the speckle background was not part of the reference. Two scenarios were studied. In secenario one, the reference was a nylon wire located at the focus of the source. In this case, the effects of scattering were considered but the spatially varying effects were not. The other scenario used a nylon wire reference from the same spatial location at which the target was located. Therefore, the spatially varying effects and scattering were taken into account.

The compressed images for the scenario when the target was located at the edge

of the -6 dB depth of field and compressed with a nylon wire target are shown in Fig. 4.16(a). The speckle before and after the target in the spatially varying Wiener filtering case appeared slightly blurry. However, the overall image excluding these regions appeared quite crisp and full of detail. Evaluating the on-axis plot in 4.16(b) it was observed that a decrease in the sidelobe levels of about 2 dB was obtained when comparing the spatially varying Wiener filtered case using a nylon target reference to the conventional Wiener filtering using a planar reflector reference. However, a large decrease in the axial resolution was visible. The spatial resolution as determined by the speckle correlation length for the conventional Wiener filter case was 902 μm. For the conventional Wiener filter case, the speckle correlation length increased by 337% when the reference changed from a planar reflector to a nylon wire target. For the spatially varying Wiener filter, the spatial resolution as determined by the correlation length was 754 μm. Overall, compressing with nylon targets as references did not improve the compression performance, regardless of whether the Wiener filter was spatially varying or not.

4.3 Spatially Varying Wiener Filter with a Spatially Varying $\overline{eSNR}$

In the original design of the REC technique [18], the compression of each scan line utilized the Wiener filter as described in (1.2) with a constant $\overline{eSNR(f)}$. $\overline{eSNR}$ (1.4) was defined as the average eSNR per frequency channel in each scan line. In this subsection, the effects of the spatially varying nature of the $\overline{eSNR}$ were evaluated. In addition, a technique to adaptively compensate for the changes in $\overline{eSNR}$ spatially in the compression scheme (Wiener filter) were examined. The overall objective is to improve the compression performance (sidelobes, spatial resolution, and eSNR) throughout the image.

4.3.1 $\overline{eSNR}$

Estimating a single $\overline{eSNR(f)}$ per scan line could be problematic in various scenarios. For example, in one scenario, one scan line could have a large amount of electronic

noise compared to other scan lines making up an image. In another example, a portion of a scan line could have a very strong specular reflection from a point target and the remaining portion of the scan line contain speckle from weak scatterers. Consequently, the specular reflector would increase the eSNR estimated for the scan line, which would in turn adjust the operating point of the Weiner filter. An increase in the eSNR would move the Weiner filter closer to an inverse filter. As a Wiener filter approaches an inverse filter the sidelobes are reduced, the resolution is improved and the noise is amplified. As a result, depending on the exact location of the operating point, the filter could be more efficient in compressing the strong specular reflector but could increase the noise in the portion of the signal with speckle only. The end result would be an image with poor quality. The image could partially be improved by adjusting the gamma parameter to shift the operating point towards a matched filter. In this scenario, the speckle portion of the signal would be above the noise floor, but the specular reflection would be characterized by larger sidelobes and a decrease in axial resolution. Therefore, to ameliorate these effects a spatially varying Wiener filter that takes into account the spatially varying nature of the eSNR was studied.

The spatially varying Wiener filter based on a spatially varying eSNR is described by the following equation:

$$\beta_{REC}(f) = \frac{V_{lin}^{'*}(f)}{|V_{lin}^{'}(f)|^2 + \gamma \overline{eSNR_0}^{-1}(f, x_0)}, \tag{4.8}$$

where $\overline{eSNR_0}$ is the echo-signal-to-noise ratio per frequency channel for the spatial region of interest defined by the axial location, x_0. $\overline{eSNR_0}$ can be described by the following expression:

$$\overline{eSNR_0(f, x_0)} = \overline{eSNR(f, x)} var(g(x_0)), \tag{4.9}$$

where the variance of the echo signal $g(x_0)$ is taken over a windowed segment using a rectangular window centered at x_0. To obtain the variance of the echo signal at location x_0, the backscattered data are compressed twice. The first compression creates a spatial map of signal strength throughout the whole image region by assuming a uniform eSNR for the scan line. From there, a map of the variance of the compressed

echoes for smaller sub-regions of the image is determined. This map is used in the spatially varying Wiener filter to adaptively select the operating point of the Wiener filter for each particular region of interest. Consequently, regions containing stronger signals will be filtered closer to an inverse filter to improve spatial resolution and sidelobe levels. Regions containing weaker echoes will be filtered closer to a matched filter to make targets visible by removing the noise at the expense of increasing the sidelobe levels and deteriorating the axial resolution. Compressing with the spatial map of eSNR can become significant when frequency-dependent attenuation is present because the image quality can be improved at all depths. The final image is constructed by stitching together each of the the compressed regions of interest.

4.3.2 Computer simulations

Computer simulations were carried out in MATLAB (Mathworks, Natick, MA) to characterize the performance of the spatially varying Wiener filter based on spatially varying maps of $\overline{eSNR}$. Computer simulations were chosen over experimental measurements in order to control image parameters more carefully. The simulations used a received pulse-echo pressure field model [93] described as

$$g'[x, y, t] = h_1(t) * f(x, y) * h_{pe}(y, t), \tag{4.10}$$

where x represents the axial spatial coordinate, y represents the lateral spatial coordinate, $f(x, y)$ is the scattering function, and $h_{pe}(y, t)$ is the modified pulse-echo spatial impulse response that takes into consideration the geometry of the transducer to the spatial extent of the scattered field (beam diffraction).

The pulse-echo impulse response, $h_1(nT, x)$, for CP was approximated by

$$h_1(t) = e^{-\frac{t^2-\tau}{\sigma_t^2}} \cos(\omega t), \tag{4.11}$$

where σ_t^2 is the second central moment of the Gaussian pulse which dictates the bandwidth of the pulse. A shift, τ, was added to $h_1(t)$ to make the pulse causal. The generated pulse-echo impulse response was located at the focus of a 2.25 MHz single-element transducer (f/4) with a -6 dB fractional bandwidth of 70%.

For REC, the impulse response function, $h_2(t)$, was constructed to have a -6 dB fractional bandwidth of 150% by gating a sinusoid of four cycles with a Hanning window

$$w(n) = \begin{cases} 0.5(1 - \cos(\frac{2\pi n}{L_H - 1})), & 0 \leq n \leq L_H - 1 \\ 0, & \text{otherwise,} \end{cases} \tag{4.12}$$

where n is an integer and L_H is the number of samples in the window. A Hanning window of length of $L_H = 96$ was used.

The spatial response for a circular focused piston source was simulated as a circular Gaussian beam, which is defined as

$$h_{pe}(y,t) = \delta(t - \frac{2R_d}{c}) e^{\frac{-y^2}{\sigma_y^2}}, \tag{4.13}$$

where R_d is the distance from the source to target in space, c is the speed of sound of the medium which was set to 1540 m/s, and σ_y is the -6 dB lateral beamwidth which is equal to 2.05 mm.

To assess the performance of the spatially varying Wiener filter, several imaging targets were evaluated. First, a simulation of a phantom S1 containing 12 point targets spaced 5 mm apart in water was evaluated. Attenuation of 2 dB $\text{MHz}^{-1}\text{cm}^{-1}$ was added to the simulation so that a decrease in backscattered energy from the point targets away from the source was achieved. Phantom S1 was evaluated for two different cases of noise floors: low noise and high noise. For the low noise case, the $eSNR$ for the region including the first point target was 62 dB. For the high noise case, the $eSNR$ in the region including the first point target was 22 dB. In the next simulation, phantom S2 was the same as the first phantom except that the wire targets were embedded in a medium producing speckle. Finally, phantom S3 contained a cystic target at the center of the phantom. Only the high noise scenario was evaluated with phantoms S2 and S3.

4.3.3 Results

The B-mode images for phantom S1 under the low noise scenario are shown in Fig. 4.17 along with an axial profile through the center of the B-mode images. Compared to CP, the B-mode images constructed using conventional REC resulted in improved axial

resolution but increases in sidelobe levels and deterioration in lateral resolution. For REC-SVWF the sidelobe levels decreased when compared to REC echoes compressed with a conventional Wiener filter. The spatial resolutions as determined by MTF for CP and for REC echoes compressed with a conventional Wiener filter and a spatially varying Wiener filter are listed in Table 4.3. Overall, the spatially varying Wiener filter had a slight degradation in axial resolution in order to improve the sidelobe levels and the eSNR. Furthermore, the amplitude of the echoes from each target was more correct with the spatially varying Wiener filter than with a conventional Wiener filter. For the conventional Wiener filter both the signal and the noise floor were boosted. The purpose of evaluating phantom S1 in a low noise environment was to show that no artifacts or significant degradation in image quality occurred.

The B-mode images for phantom S1 under the high noise scenario are shown in Fig. 4.18 along with an axial profile through the center of the B-mode images. In the high noise scenario, the spatially varying Wiener filter allowed the operating point of the Wiener filter to remain at the same operating point as in the low-noise scenario. Consequently, when using the spatially varying Wiener filter the axial resolution was nearly the same as in the low noise scenario with the added benefit that the noise floor was pushed below the dynamic range of the image. In the scenario where a conventional Wiener filter was used for compression in the high noise case, the γ parameter was adjusted until the noise was removed. This adjustment increased sidelobe levels and degraded the axial resolution in order to improve the eSNR. Therefore, the benefits of the spatially varying Wiener filter were clearly observed in this case. The spatial resolution as determined by MTF for CP and for REC echoes compressed with a conventional Wiener filter and a spatially varying Wiener filter are listed in Table 4.4. Similar to the low noise case, the spatially varying Wiener filter had a slight degradation in axial resolution in order to improve the sidelobe levels and the eSNR. Overall, the results for phantom S1 suggested that the spatially varying Wiener filter improved the image quality over CP and REC using with a conventional Wiener filter.

The B-mode images for phantom S2 under the high noise scenario are shown in Fig. 4.19 an axial profile through the center of the B-mode images. In the REC case shown in Fig. 4.19(a), i.e., echoes compressed with a conventional Wiener filter, the point

targets that were further away from the source became blurry in the image. The blurry targets were a result of the effects of frequency-dependent attenuation that decreased the eSNR as a function of depth. Consequently, the γ parameter forced the operating point of the Wiener filter towards an inverse filter in order to reduce sidelobe levels and obtain improved resolution at the expense of boosting the noise. The noise boost degraded the image as the imaging depth increased. When compared to CP, the results obtained with conventional REC were still a slight improvement because of the increased depth of penetration into phantom S2. However, when using the spatially varying Wiener filter, results were further improved by reducing the amount of blur in the speckle at depths greater than 60 mm. The spatially varying Wiener filter was adjusting the operating point as a function of depth as the eSNR was decreasing. Therefore, the spatially varying Wiener filter improved results by reducing the amount of blurring of speckle at depths greater than 60 mm. However, the tradeoff was that a degradation in axial resolution was obtained and a slight increase in sidelobe levels was observed at these depths. Overall, the spatially varying Wiener filter applied on phantom S2 showed promising results as image quality improved at depths where CP had low eSNR and conventional REC contained a large amount of noise and sidelobes.

Finally, phantom S3 was evaluated under the high noise scenario. The B-mode images for phantom S3 under the high noise scenario are shown in Fig. 4.20 an axial profile through the center of the B-mode is shown in Fig. 4.21. Phantom S3 consisted of a cystic target surrounded by tissue-mimicking material. The cystic target evaluated was equivalent to a fluid-filled target with no internal scattering objects. Therefore, the only backscattered signal present in that region would be additive noise. By applying a spatially varying Wiener filter, the noise in the cystic region could be removed by shifting the operating point of the Wiener filter towards a matched filter. With conventional Wiener filtering the cystic region is smeared by either sidelobes or noise. Consequently, the dimensions of the cystic target became much smaller. This could potentially be a problem if the region was small because the sidelobes and noise could mask the region. Therefore, the results of the spatially varying Wiener filter compression scheme for this target clearly displayed the benefit of using a spatially varying Wiener filter. Note that in this simulation there was no attenuation present; therefore, the amplitude did

not decrease with increasing depth. However, with the spatially varying Wiener filter the speckle appeared to have increased because regions that were buried in noise using conventional Wiener filtering and CP were now anechoic and noise-free. To quantify the improvement using the spatially varying Wiener filter, the CNR metric was applied to obtain a measure of contrast between the cyst and the background region. CNR for CP was 1.69. For REC, the CNR was 1.92 and 3.29 for the conventional Wiener filter and the spatially varying Wiener filter, respectively. Overall, the spatially varying Wiener filter based on spatially varying maps of the signal-to-noise ratio significantly improved image quality by increasing the contrast when compared to CP and REC echoes compressed with a conventional Wiener filter.

4.4 Conclusion

In this chapter several spatially varying Wiener filters were evaluated. Initially, a spatially varying Wiener filter that corrects for diffraction effects locally was tested. It was observed that the spatially varying Wiener filter worked for large specular objects such as a planar reflector. Moreover, another spatially varying Wiener filter was implemented that corrects for scattering effects locally as evaluated in the wire target study. The conclusion of that study was that the spatially varying Wiener filter based on planar references offered little help at improving the compression performance. Therefore, the new filter was limited in improving only planar-surface-like targets and not targets with curved surfaces.

Furthermore, another spatially varying Wiener was evaluated by correcting for both scattering and diffraction locally. Under this spatially varying Wiener filter, it was established that improved results were obtained because of self-compression. Self-compression is not easily implementable as frequency-dependent scattering because the object function must be known to account for scattering-dependent effects.

Finally, the most promising spatially varying Wiener filter evaluated corrected for $\overline{eSNR}$ locally to improve compression performance. Specifically, the eSNR was increased in deeper areas imaged at the expense of a small degradation in spatial resolution and slight increase in sidelobe levels. Images of wire targets and anechoic lesion were observed to improve in simulations compared to conventional methods of imaging.

4.5 Figures and Tables

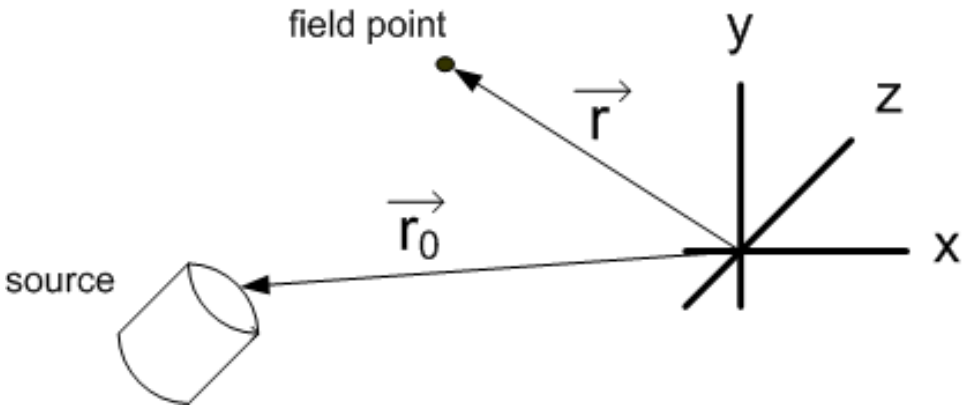

Figure 4.1: Description of coordinate system for calculation of spatial impulse responses.

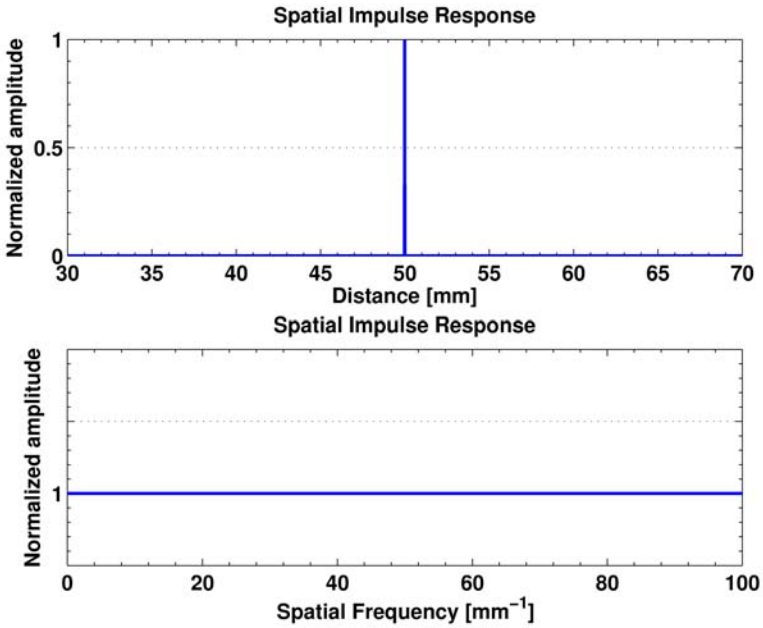

Figure 4.2: Spatial impulse response as a function of distance and as function of spatial frequency for a 2.25 MHz (f/3) source. The field point is located at the focus, i.e., $x = 0$, $y = 0$, and $z = 50$ mm.

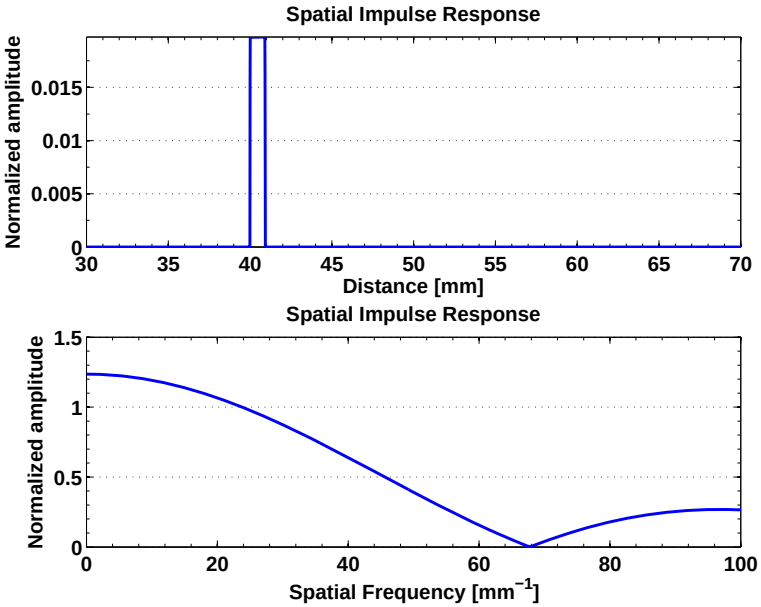

Figure 4.3: Spatial impulse response as a function of distance and as function of spatial frequency for a 2.25 MHz (f/3) source. The field point is located 10 mm before the focus, i.e., $x = 0$, $y = 0$, and $z = 40$ mm. These plots have been normalized with respect to the spatial impulse response at the focus.

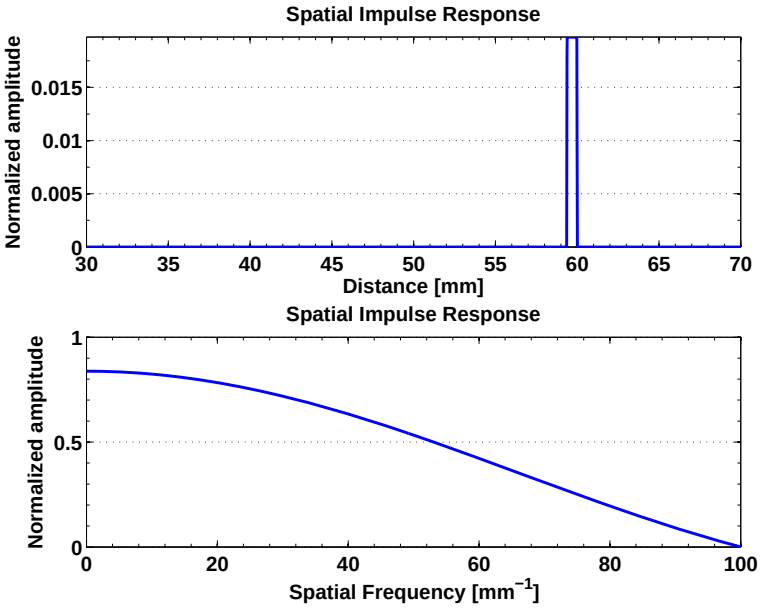

Figure 4.4: Spatial impulse response as a function of distance and as function of spatial frequency for a 2.25 MHz (f/3) source. The field point is located 10 mm after the focus, i.e., $x = 0$, $y = 0$, and $z = 60$ mm. These plots have been normalized with respect to the spatial impulse response at the focus.

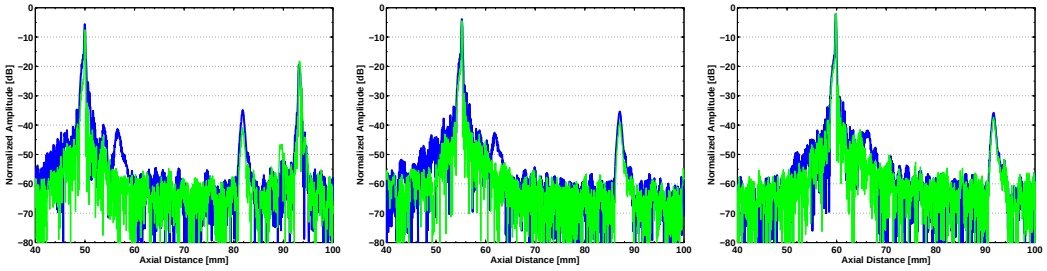

(a) @ -6 dB amplitude before the focus (b) @ -4 dB amplitude before the focus (c) @ -2 dB amplitude before the focus

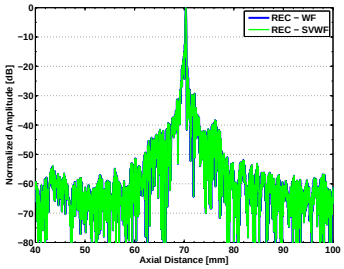

(d) @ focus

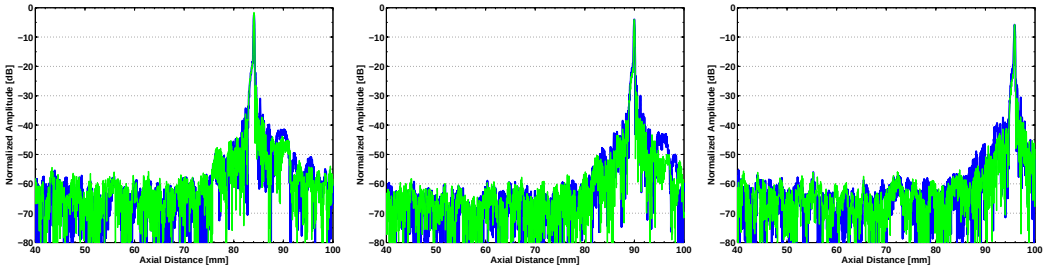

(e) @ -2 dB amplitude after the focus (f) @ -4 dB amplitude after the focus (g) @ -6 dB amplitude after the focus

Figure 4.5: The compression results from a spatially varying Wiener filter (SVWF) versus a conventional Wiener filtering (WF) at various locations throughout the depth of field.

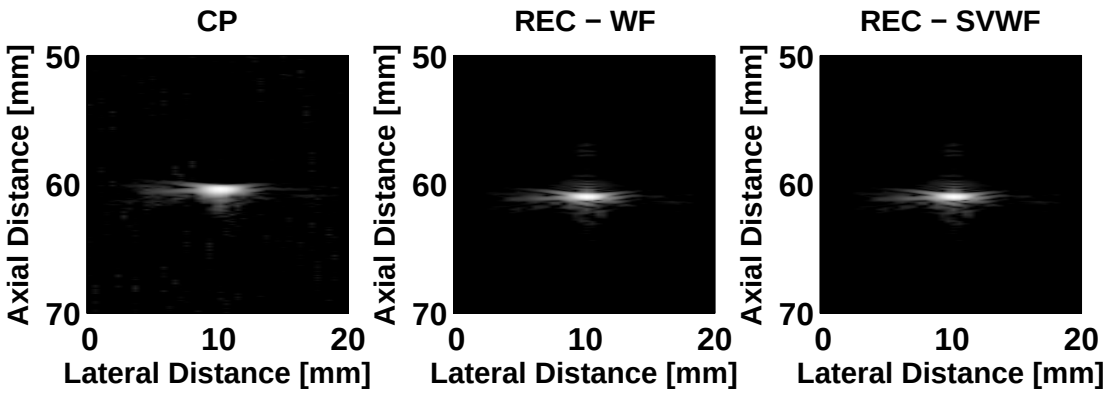

(a)

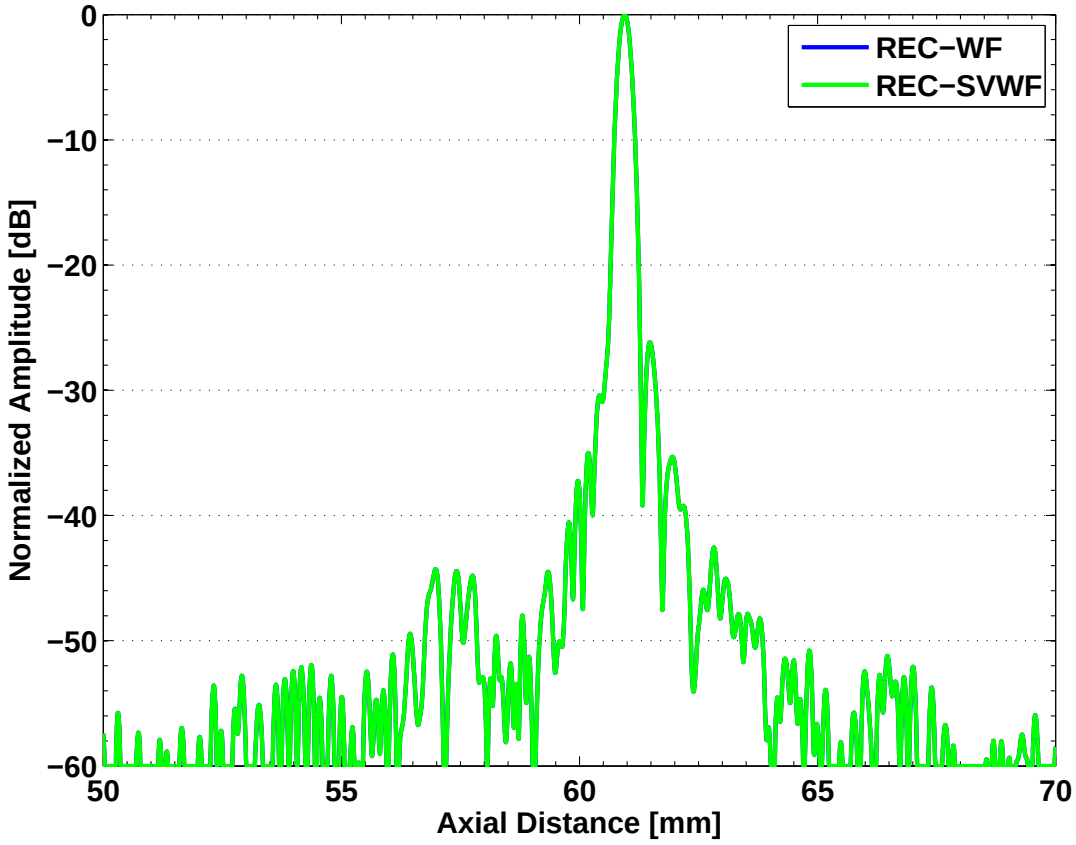

(b)

Figure 4.6: (a) B-mode image and (b) on-axis plot of a 100 μm tungsten wire target located at the focus for both conventional Wiener filtering (WF) and spatially varying Wiener filtering (SVWF). Image dynamic range = -50 dB.

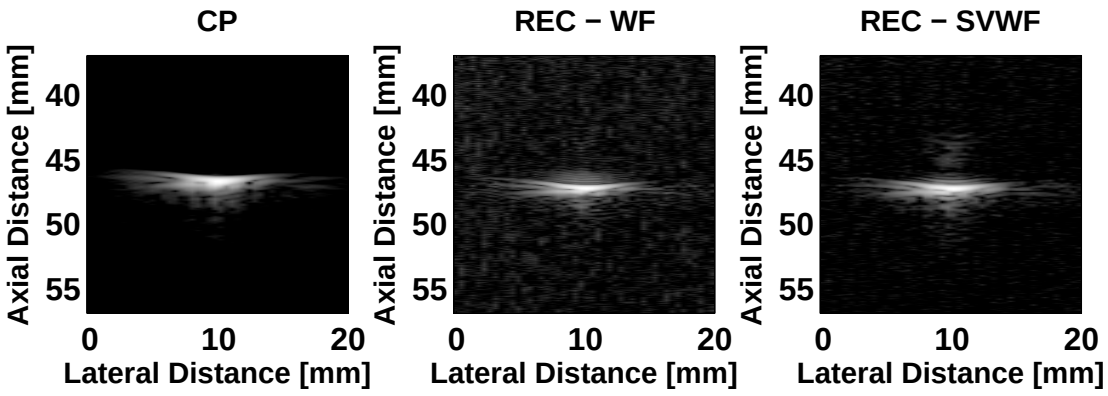

(a)

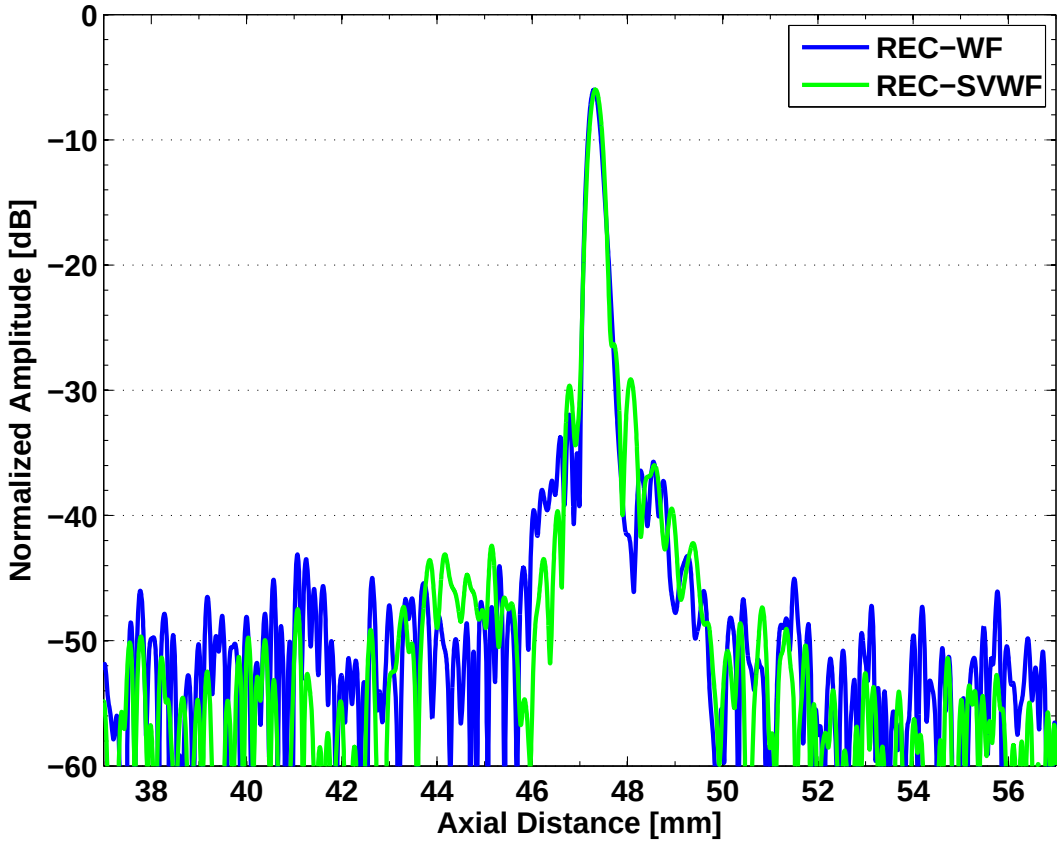

(b)

Figure 4.7: (a) B-mode image and (b) on-axis plot of a 100 μm tungsten wire target located at -6 dB amplitude point before the focus for both conventional Wiener filtering (WF) and spatially varying Wiener filtering (SVWF). Image dynamic range = -50 dB.

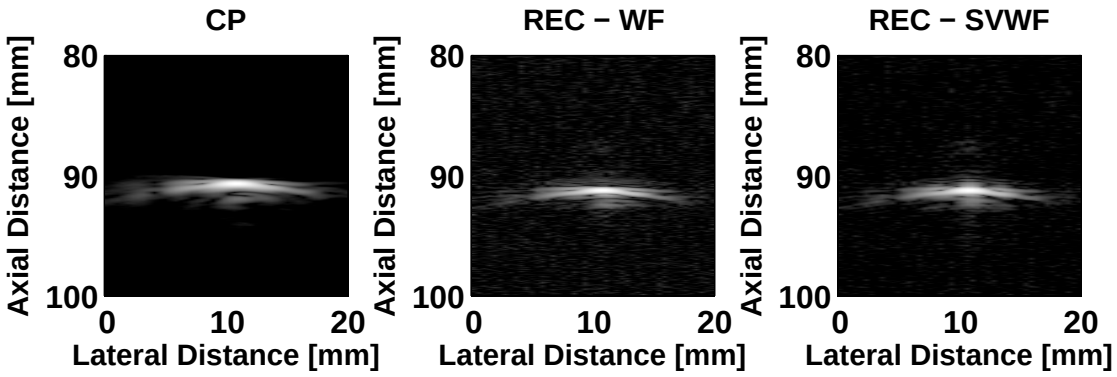

(a)

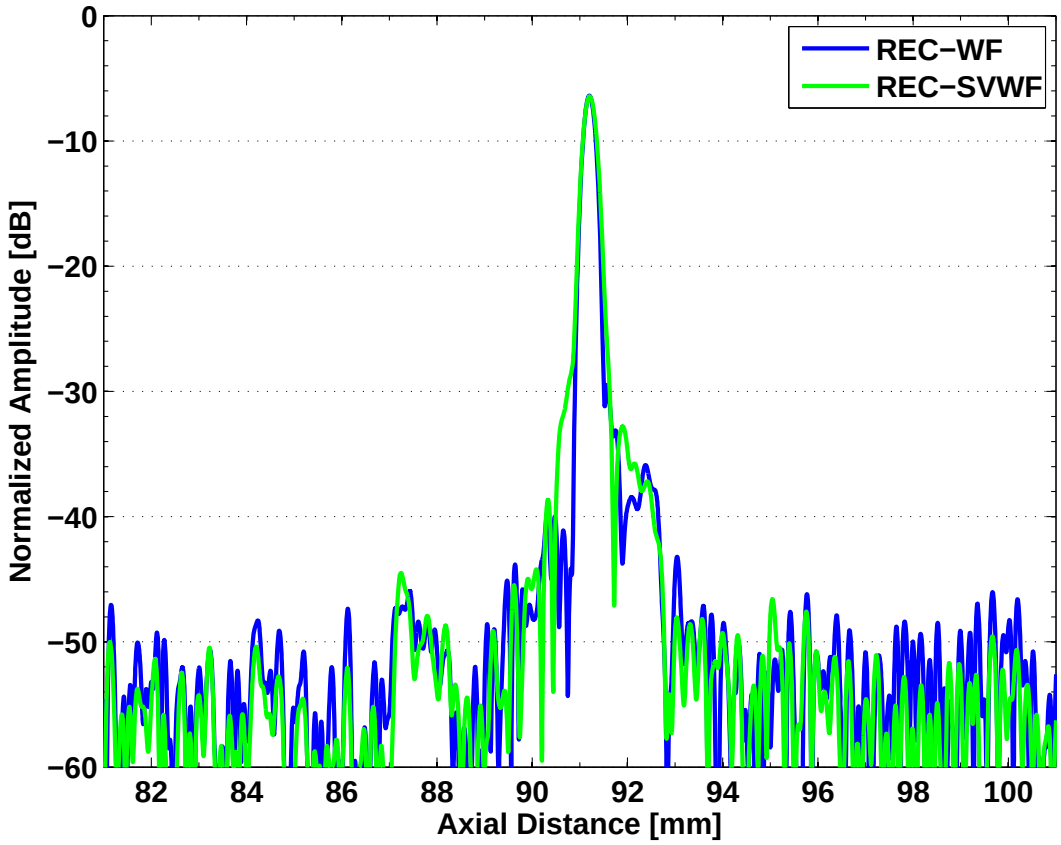

(b)

Figure 4.8: (a) B-mode image and (b) on-axis plot of a 100 μm tungsten wire target located at -6 dB amplitude point after the focus for both conventional Wiener filtering (WF) and spatially varying Wiener filtering (SVWF). Image dynamic range = -50 dB.

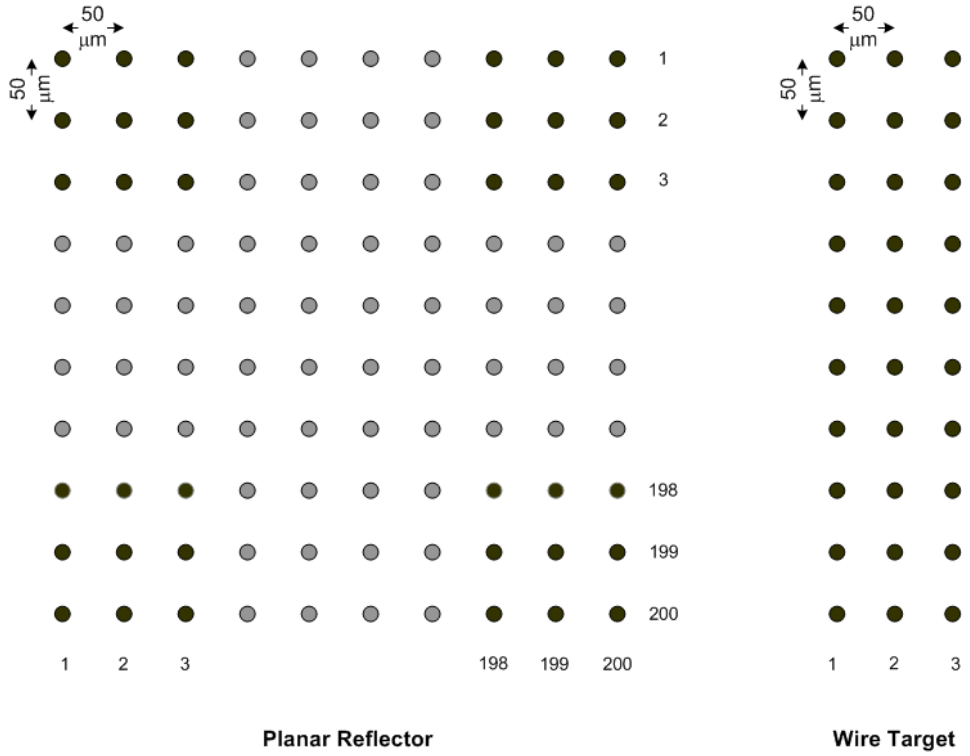

Figure 4.9: Input grid used for planar reflector and wire target in Field II simulations.

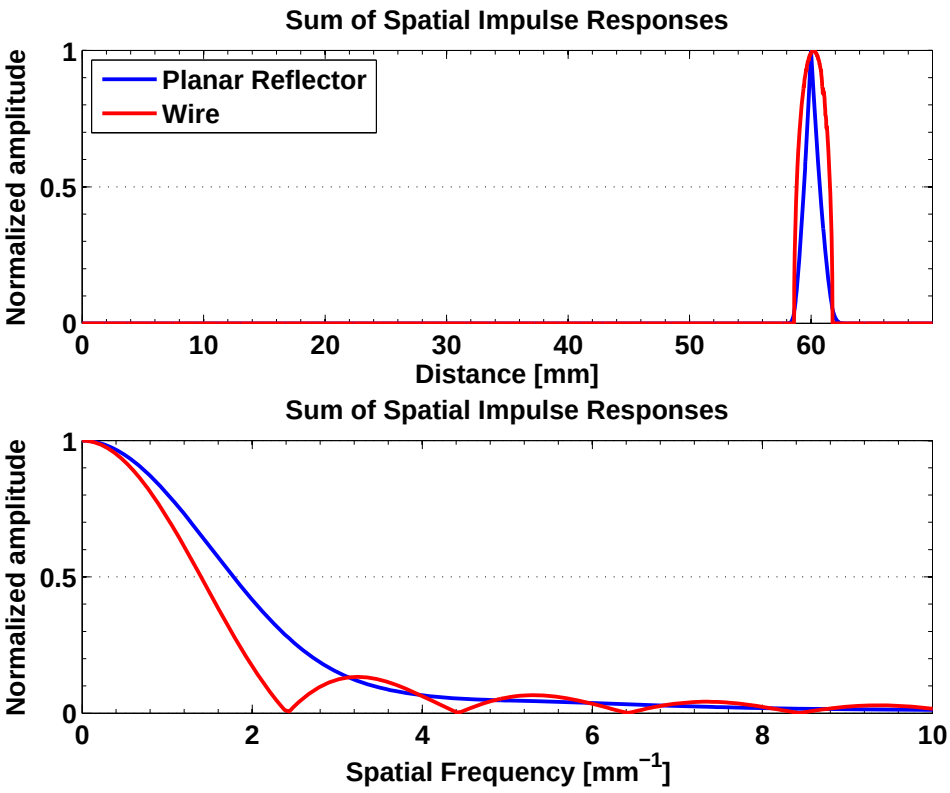

Figure 4.10: Sum of the spatial impulse response from each grid point as a function of distance and as function of spatial frequency for a 2.25 MHz (f/3) source with a focal depth of 60 mm for planar reflector (blue) and a wire target (red). These plots have been normalized to their respective maximum amplitude for shape comparison. The ratio of maximum amplitude between the wire and planar reflector was 0.82%.

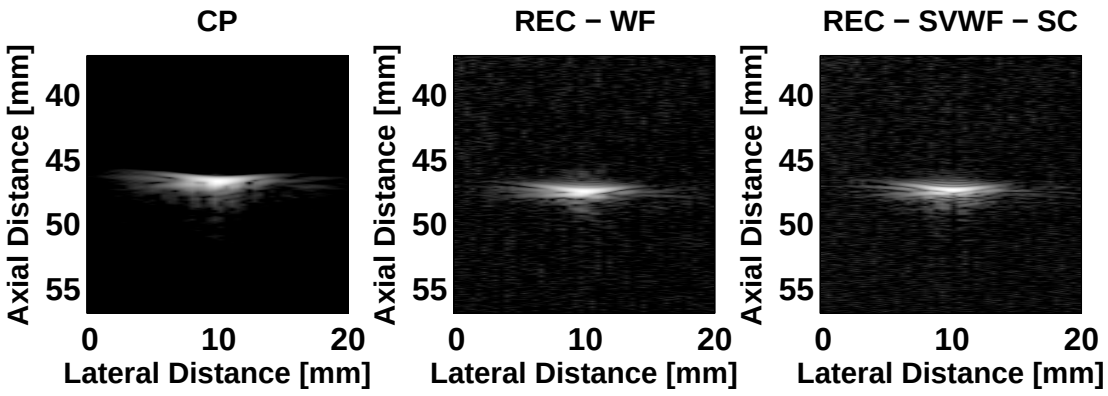

(a)

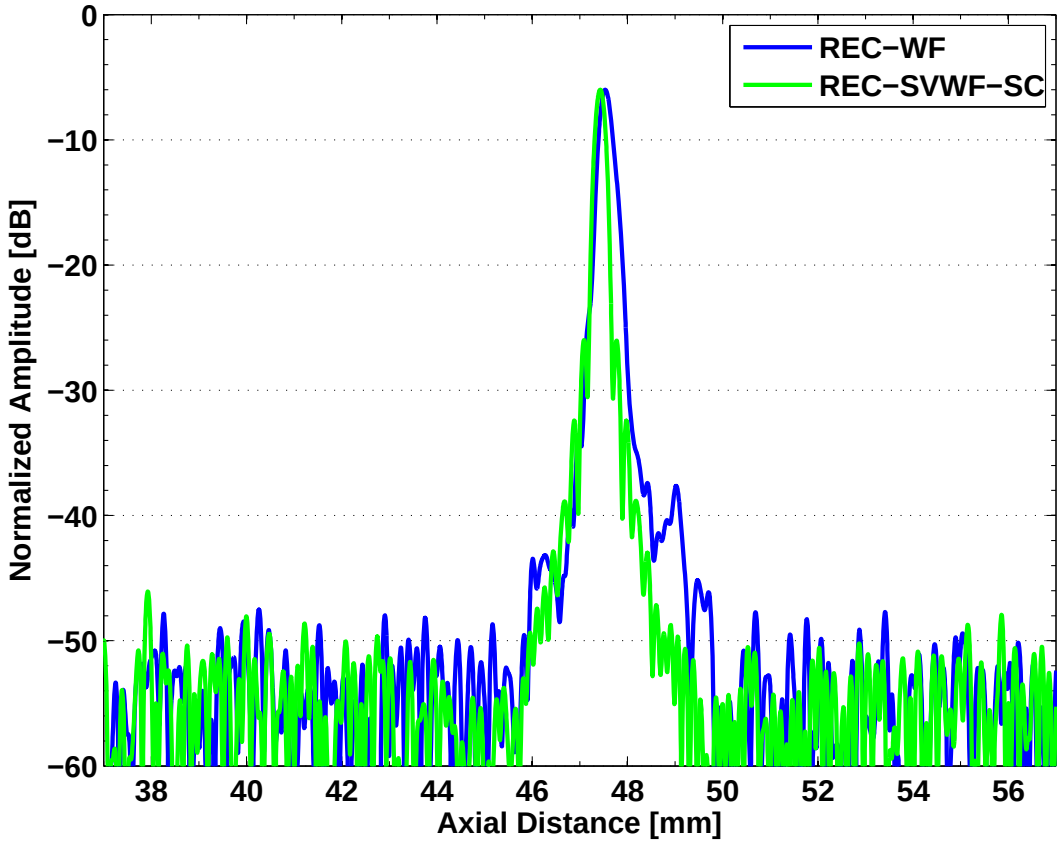

(b)

Figure 4.11: (a) B-mode image and (b) on-axis plot of a 100 μm tungsten wire target located at the edge of -6 dB depth of field before the focus for both conventional Wiener filtering (WF) and spatially varying Wiener filtering (SVWF). In this case, WF identifies echoes that have been compressed with a tungsten wire target located at the focus. SVWF-SC identifies echoes that have been self-compressed (i.e., the reference is from a tungsten wire located at the same depth the target was imaged). Image dynamic range = -50 dB.

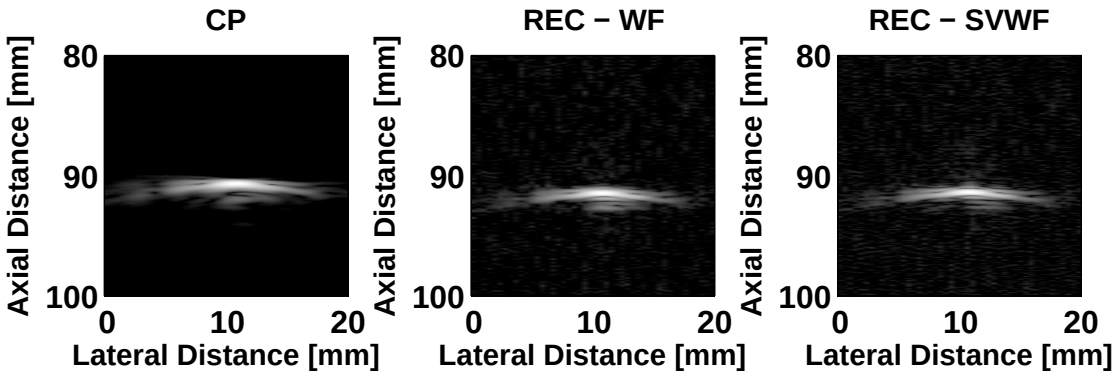

(a)

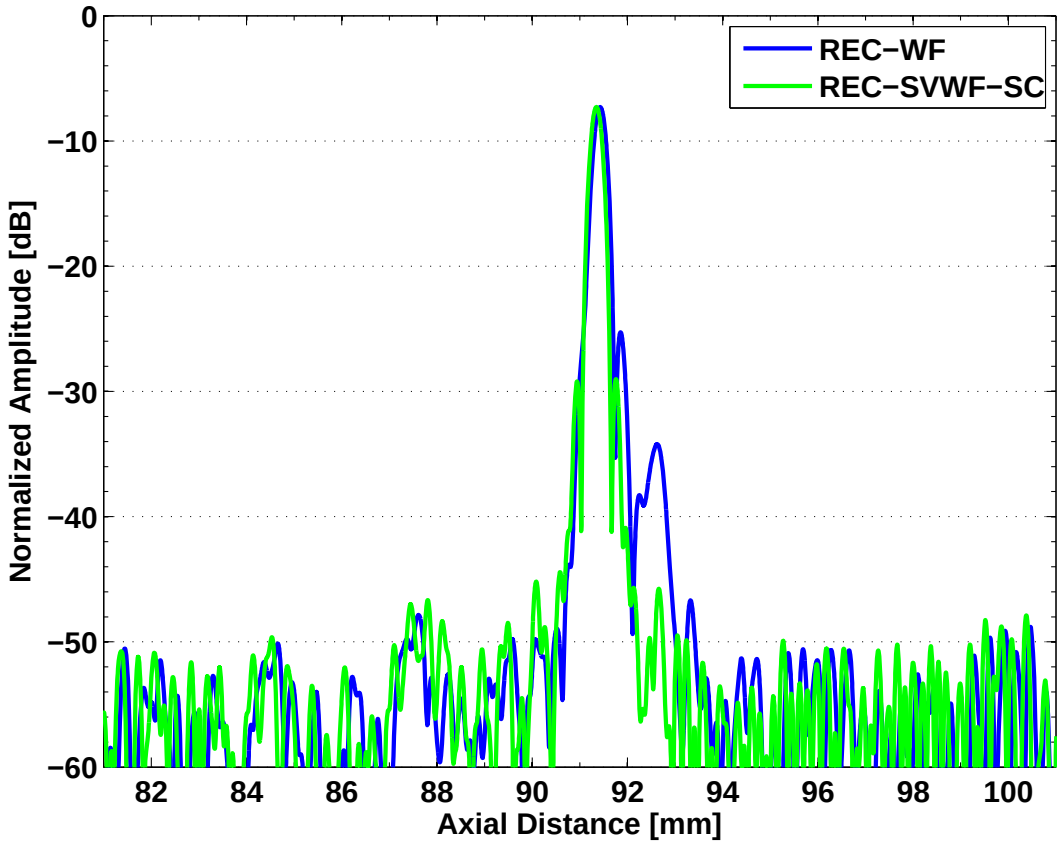

(b)

Figure 4.12: (a) B-mode image and (b) on-axis plot of a 100 μm tungsten wire target located at the edge of the -6 dB depth of field after the focus. In this case, WF identifies echoes that have been compressed with a tungsten wire target located at the focus. SVWF-SC identifies echoes that have been self-compressed (i.e., the reference is from a tungsten wire located at the same depth the target was imaged). Image dynamic range = -50 dB.

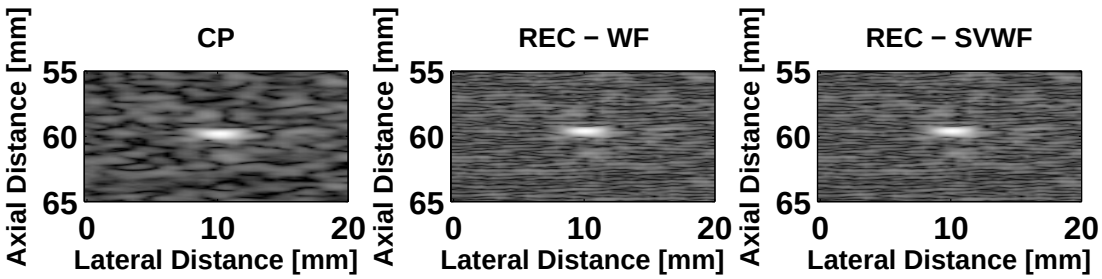

(a)

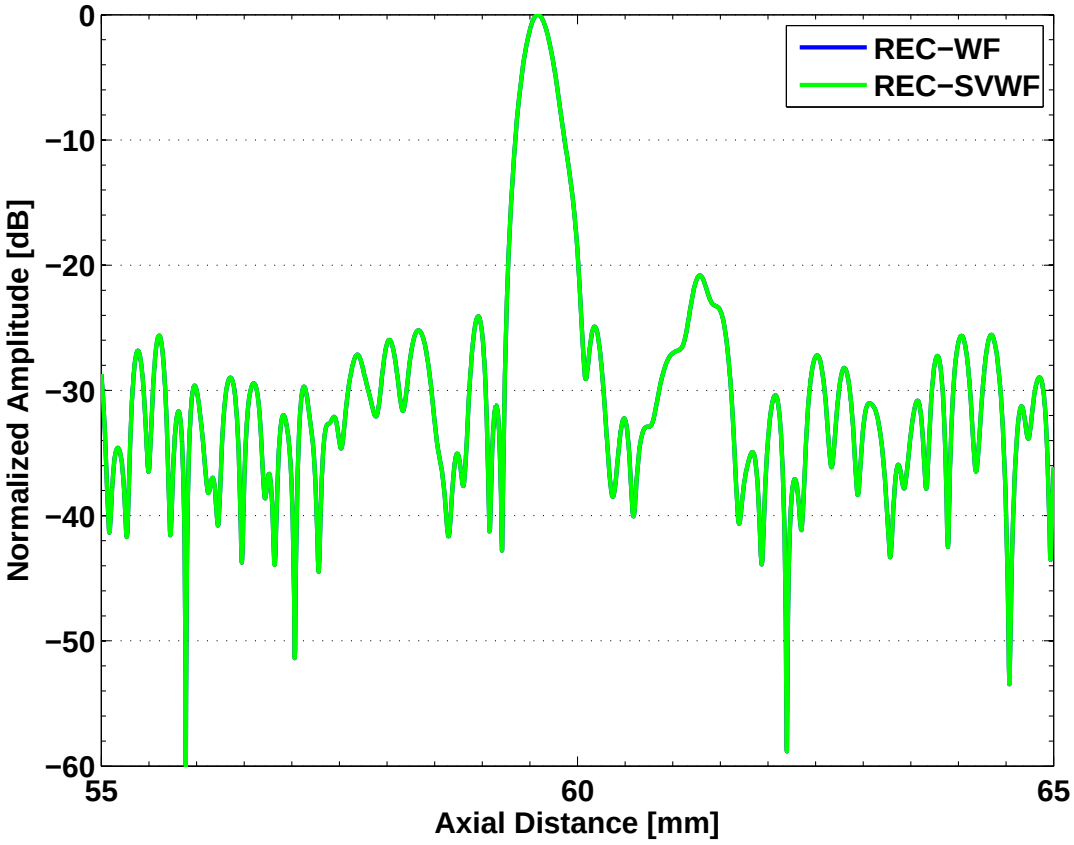

(b)

Figure 4.13: (a) B-mode image and (b) on-axis plot of a 120 μm ATS nylon wire target located at the focus for both conventional Wiener filtering (WF) and spatially varying Wiener filtering (SVWF). Image dynamic range = -50 dB.

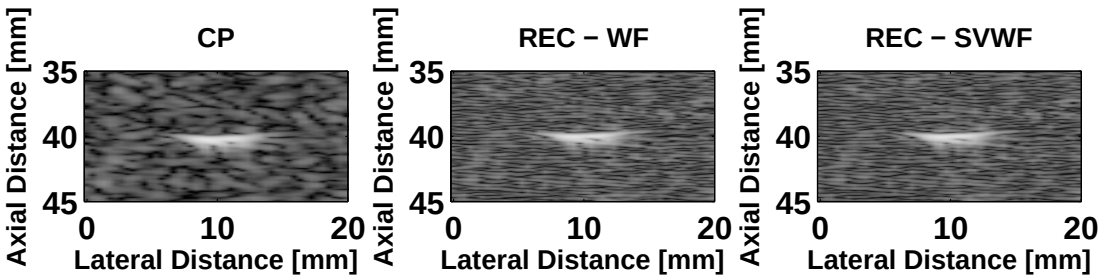

(a)

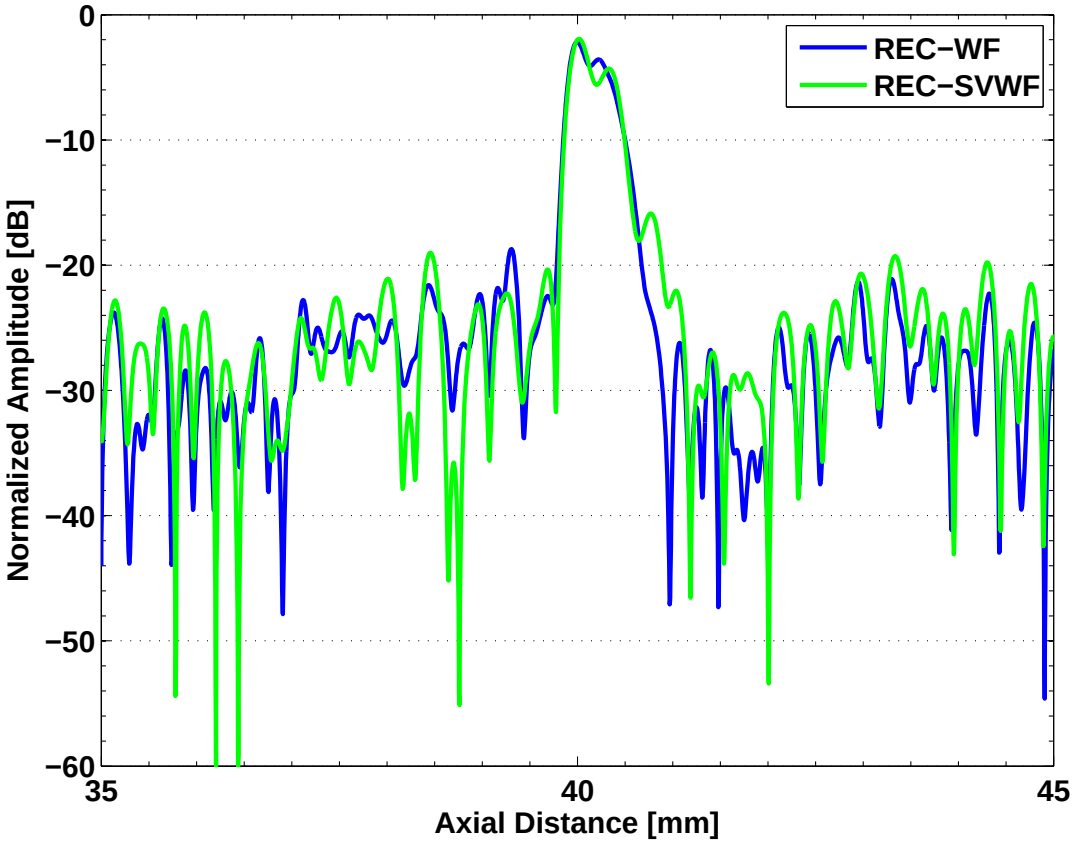

(b)

Figure 4.14: (a) B-mode image and (b) on-axis plot of a 120 μm ATS nylon wire target located at the edge of the -6 dB depth of field prior to the focus for both conventional Wiener filtering (WF) and spatially varying Wiener filtering (SVWF). Image dynamic range = -50 dB.

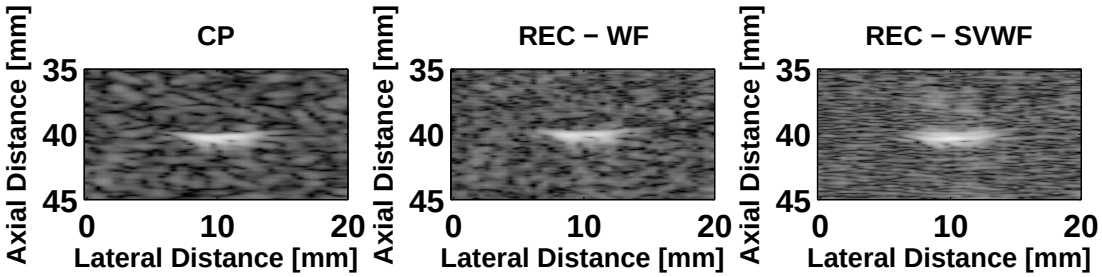

(a)

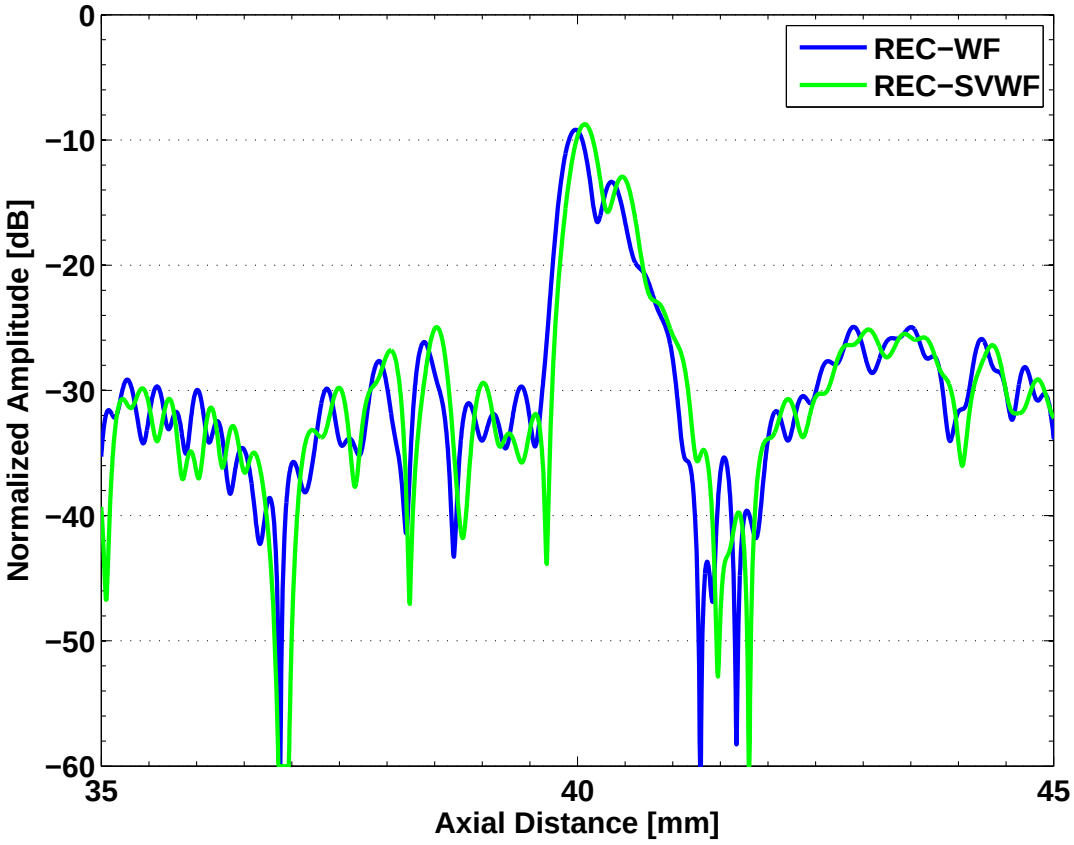

(b)

Figure 4.15: (a) B-mode image and (b) on-axis plot of a 120 μm ATS nylon wire target located at the edge of the -6 dB depth of field before the focus for both conventional Wiener filtering (WF) and spatially varying Wiener filtering (SVWF). In this case, WF refers to the echoes have been compressed with a tungsten wire target that was located at the focus. SVWF refers to the echoes have been compressed with a reference target obtained at the same spatial location (the reference is from a tungsten wire). Image dynamic range = -50 dB.

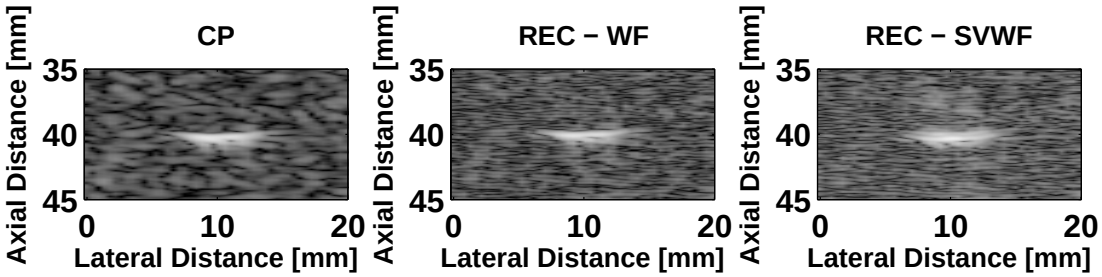

(a)

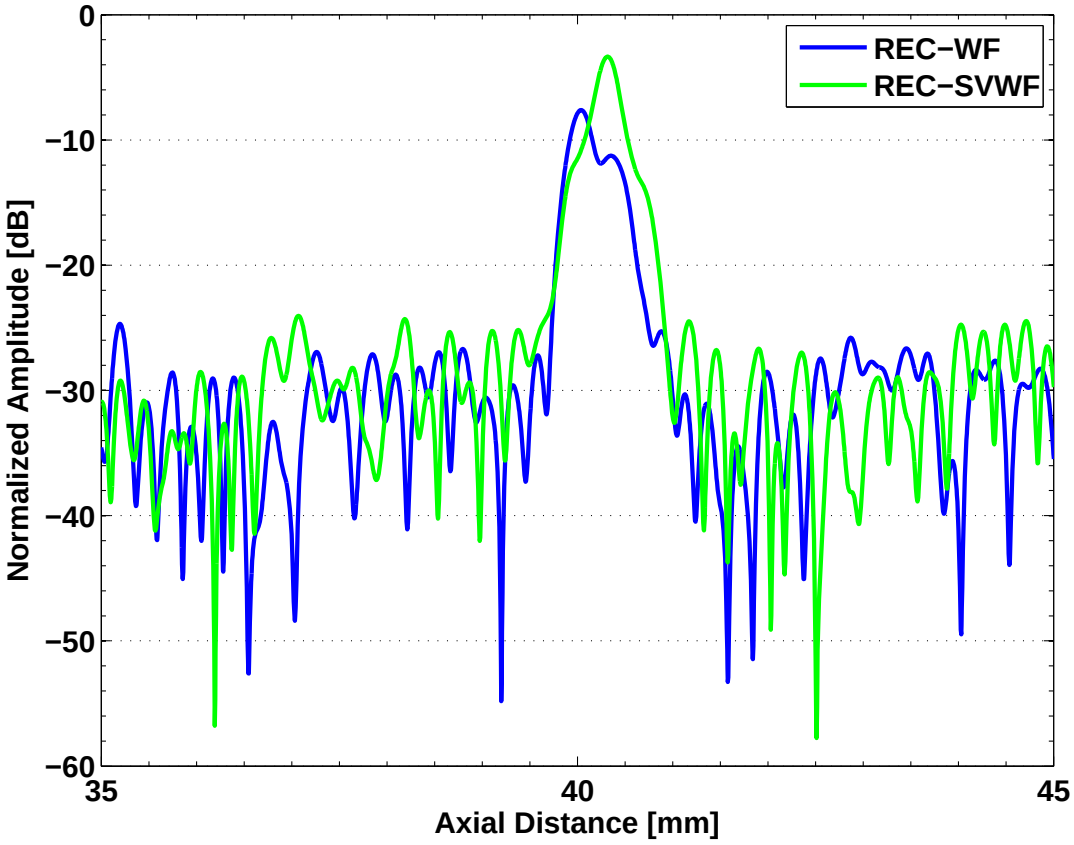

(b)

Figure 4.16: (a) B-mode image and (b) on-axis plot of a 120 μm ATS nylon wire target located at the edge of the -6 dB depth of field before the focus for both conventional Wiener filtering (WF) and spatially varying Wiener filtering (SVWF). In this case, WF refers to the echoes have been compressed with a nylon wire target that was located at the focus. SVWF refers to the echoes have been self-compressed (i.e., the reference is from a nylon wire located at the same depth the target was imaged). Image dynamic range = -50 dB.

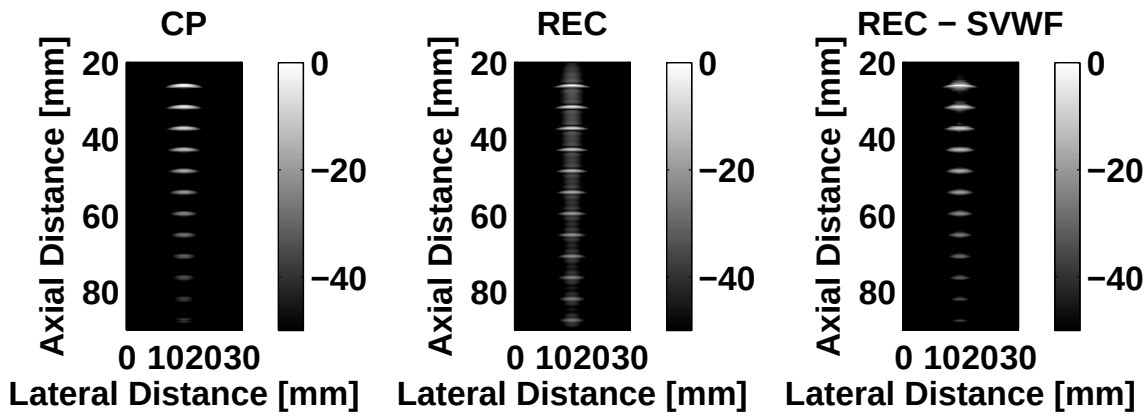

(a)

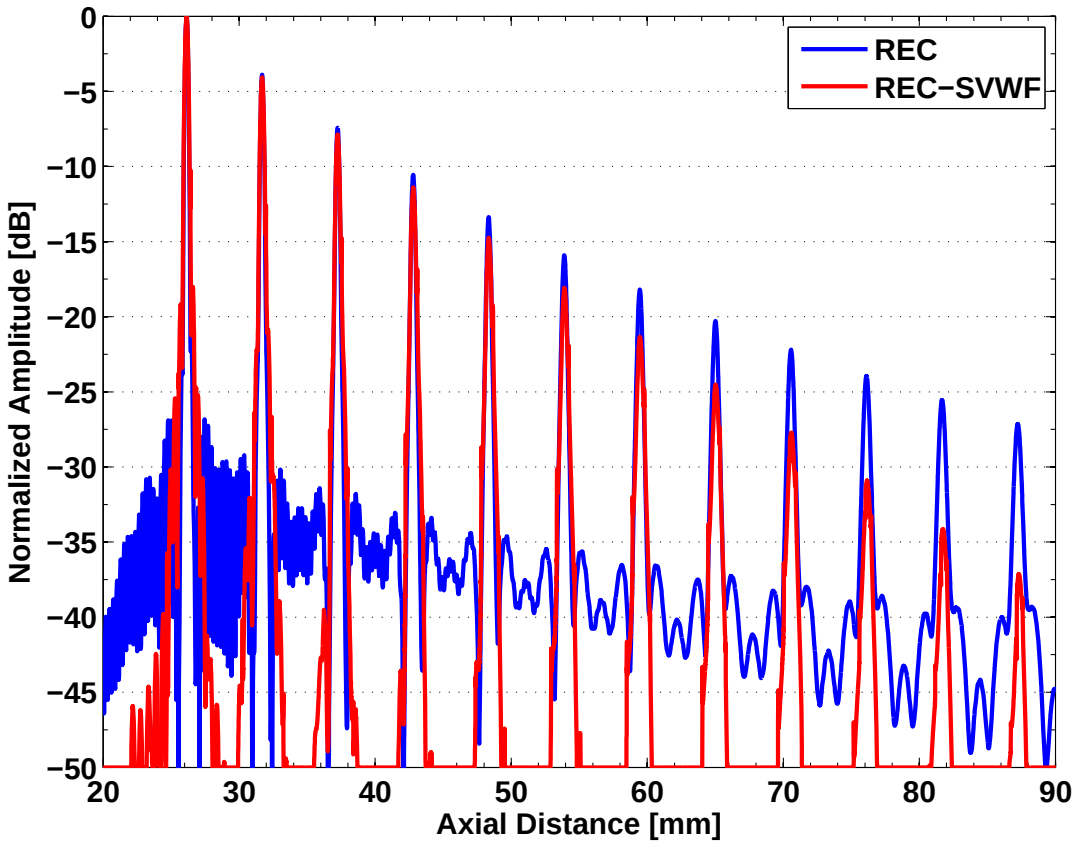

(b)

Figure 4.17: (a) B-mode image and (b) on-axis plot of 12 wire targets for CP, REC and REC-SVWF for a low noise scenario.

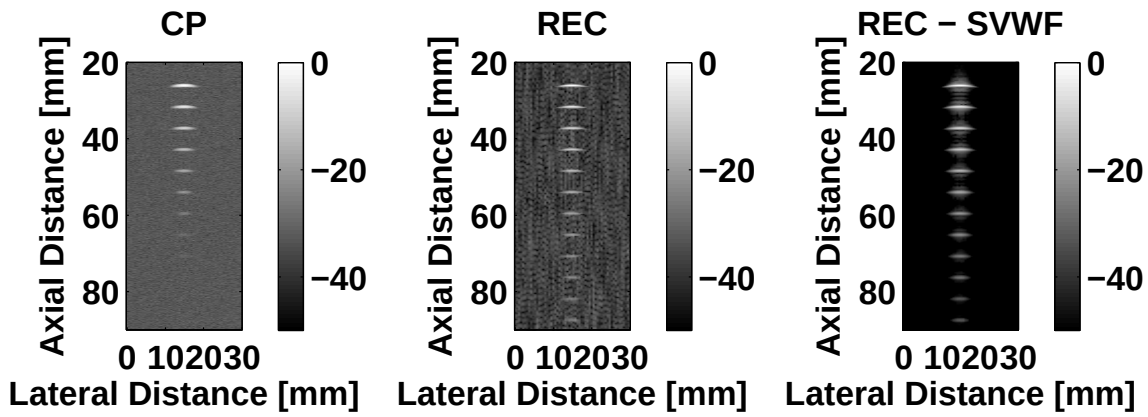

(a)

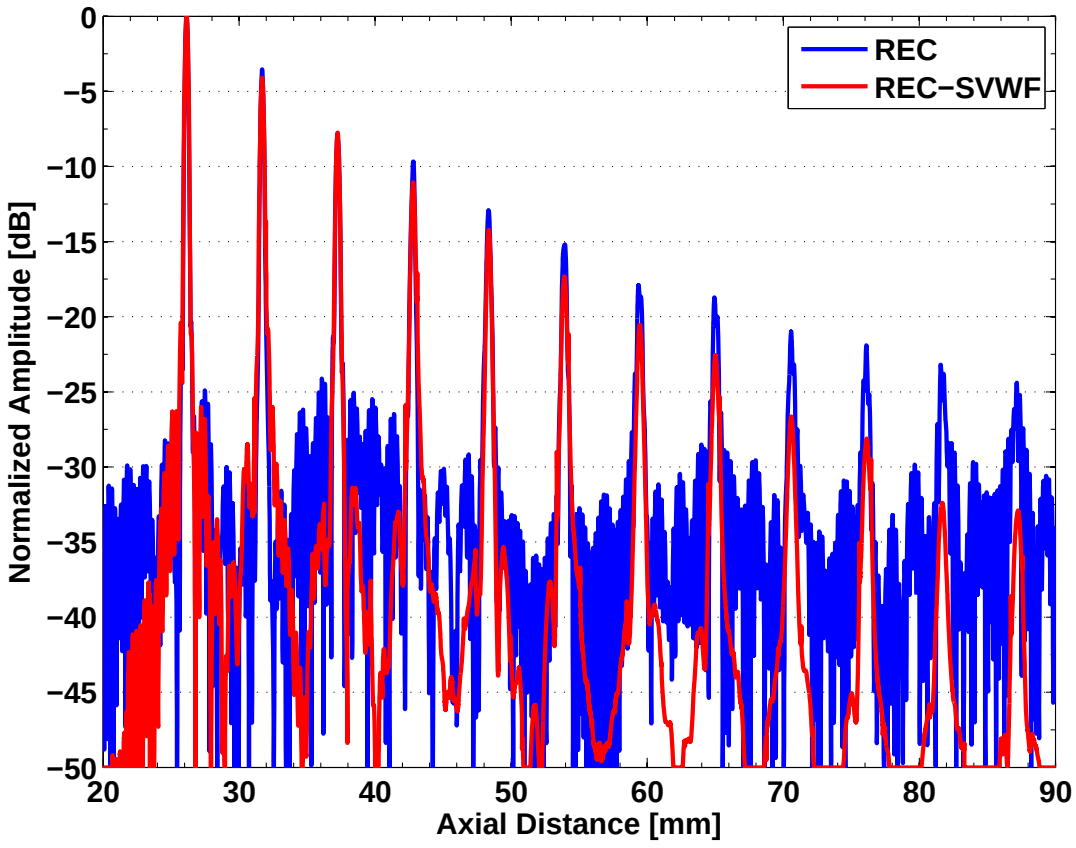

(b)

Figure 4.18: (a) B-mode image and (b) on-axis plot of 12 wire targets for CP, REC and REC-SVWF for a high noise scenario.

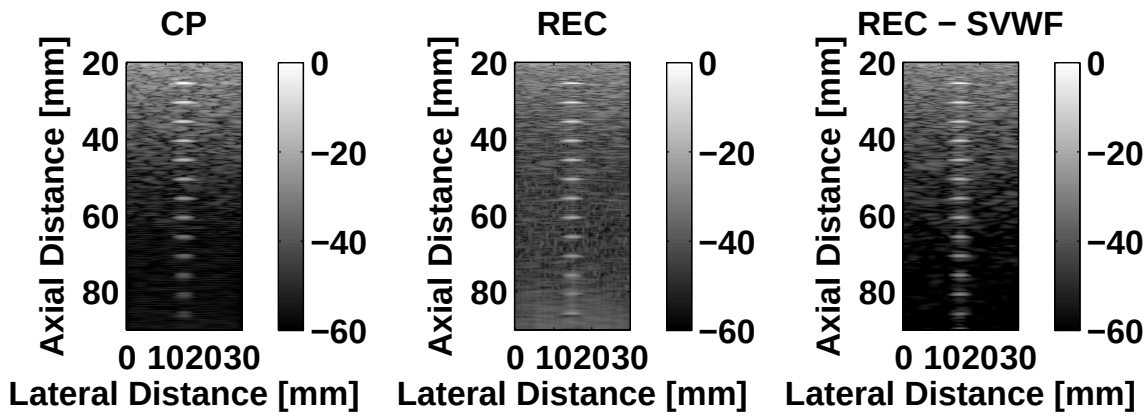

(a)

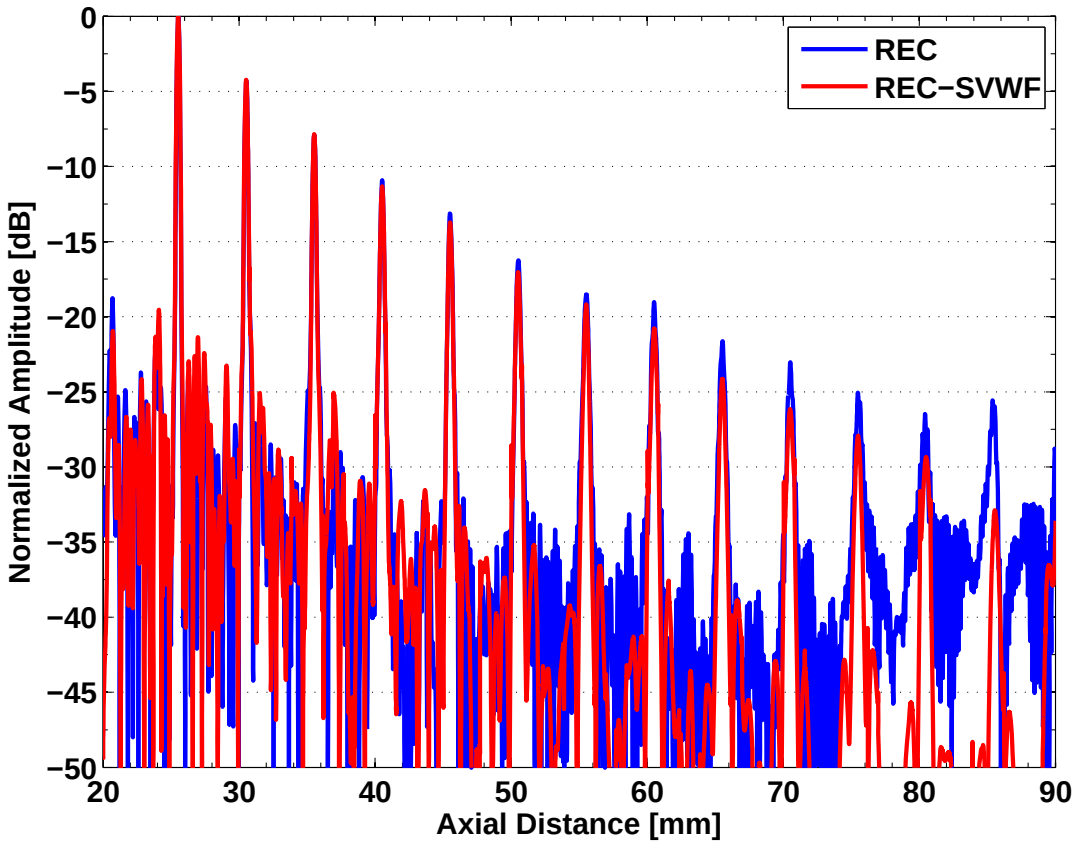

(b)

Figure 4.19: (a) B-mode image and (b) on-axis plot of 12 wire targets buried in tissue-mimicking material for CP, REC and REC-SVWF.

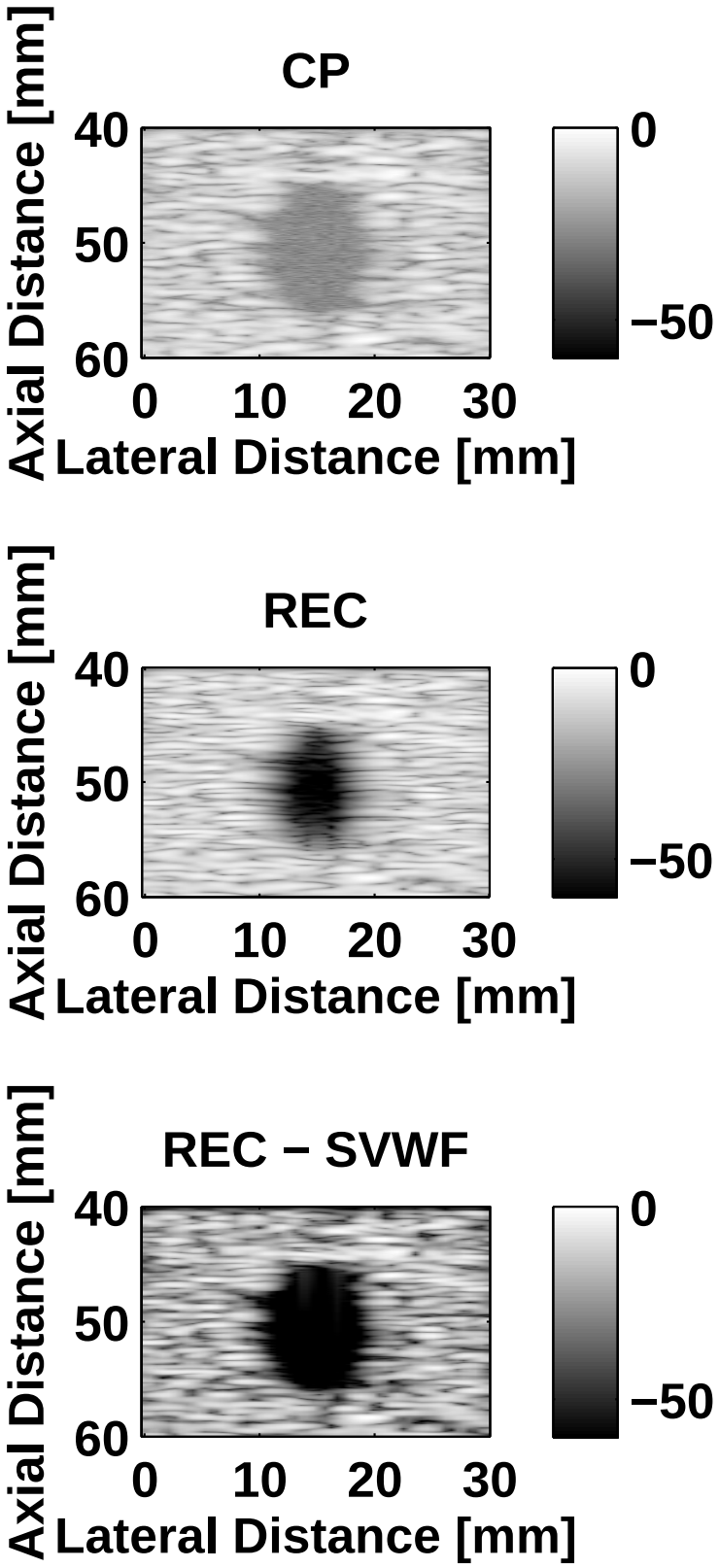

Figure 4.20: B-mode image of a cystic target surrounded by tissue-mimicking material for CP, REC and REC-SVWF.

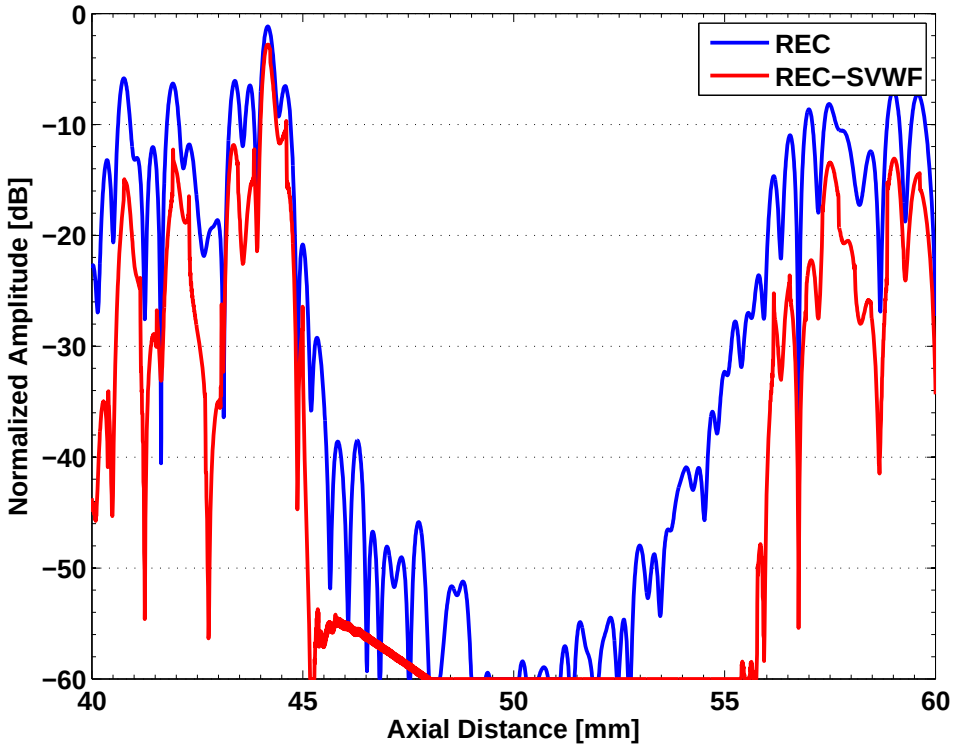

Figure 4.21: On-axis plot of a cystic target surrounded by tissue-mimicking material for REC and REC-SVWF.

Table 4.1: Axial resolution estimates from the MTF for the two compressed outputs: conventional Wiener filtering (WF) and spatially varying Wiener filtering (SVWF) along with CP as a reference for the planar reflector target.

Location	REC-WF (μm)	REC-SVWF (μm)	CP (μm)
-6-dB amplitude before focus	440.3	300.4	431.1
-4-dB amplitude before focus	413.4	301.1	451.7
-2-dB amplitude before focus	346.5	303.4	451.7
focus	302.0	302.0	421.0
-2-dB amplitude after focus	311.9	301.9	420.6
-4-dB amplitude after focus	331.5	301.9	437.2
-6-dB amplitude after focus	376.5	301.2	450.1

Table 4.2: Spatial resolution values determined from the MTF for the conventional Wiener filtering (WF), and the spatially varying Wiener filtering (SVWF). Two different types of references were used: planar reflector and wire target (self-compression). CP results are shown as a reference for the tungsten wire target.

	Reference				
	Planar		Wire		
Location	REC-WF (μm)	REC-SVWF (μm)	REC-WF (μm)	REC-SVWF (μm)	CP (μm)
-6 dB amplitude					
before focus	396.0	426.4	489.8	338.8	569.9
focus	426.4	426.4	434.0	434.0	508.2
-6 dB amplitude					
after focus	422.1	470.9	417.7	412.1	510.3

Table 4.3: Spatial resolution values determined from the MTF for REC with conventional Wiener filtering (WF) and spatially varying Wiener filtering (SVWF) along with CP as a reference for the tungsten wire target. These results are for the low noise scenario.

Target #	REC-WF (μm)	REC-SVWF (μm)	CP (μm)
1	368.9	392.6	658.1
2	401.7	424.8	667.5
3	442.2	458.1	687.1
4	491.8	502.4	718.8
5	554.0	543.3	876.1
6	623.0	581.6	824.5
7	690.5	591.5	910.2
8	753.6	922.1	1015.8
9	839.7	973.4	1121.4
10	922.2	1070.0	1274.3
11	1008.5	1240.5	1430.3
12	1103.7	1103.7	1592.8

Table 4.4: Spatial resolution values determined from the MTF for REC with conventional Wiener filtering (WF) and spatially varying Wiener filtering (SVWF) along with CP as a reference for the tungsten wire target. These results are for the high noise scenario.

Target #	REC-WF (μm)	REC-SVWF (μm)	CP (μm)
1	379.8	388.3	658.1
2	407.5	422.2	667.5
3	443.6	461.1	687.1
4	537.1	526.9	718.8
5	631.4	556.2	876.1
6	697.3	622.9	824.5
7	697.4	640.1	910.2
8	805.6	922.1	1015.8
9	1112.5	881.6	1121.4
10	960.1	1062.0	1274.3
11	1649.1	1158.5	1430.3
12	5607.0	1103.7	1592.8